Spectro-photometric properties of galaxies in the nearby Universe

Òscar Maireles González

Advisor: Jairo Méndez Abreu

Master Astrofísica 2019 - 2020

Index

Abstract

El objetivo de este trabajo es realizar una descomposición espectro-fotométrica de un conjunto de galaxias barradas para así poder estudiar sus poblaciones estelares y hacer un análisis estadístico de las propiedades de esas galaxias.

Para llevar a cabo esta tarea se hará uso del software C2D, que a su vez utiliza GASP2D, ambos escritos en lenguaje IDL y desarrollados por Méndez-Abreu et al. (2008, 2014, 2019). Este código ya se ha probado en galaxias con dos componentes (bulbo+disco) con resultados satisfactorios. El siguiente paso a llevar a cabo con este código ha sido el de añadir la barra como una tercera componente sobre la que hacer la descomposición espectro-fotométrica. La modelización de los perfiles de luz de cada componente se ha llevado a cabo mediante las ecuaciones 2, 4 y 5, en la Sección 3.2, que corresponden a un perfil de Sérsic para el bulbo, una función exponencial que se adapta a los posibles tipos de discos y la proyección en dos dimensiones de un elipsoide de Ferrers en tres dimensiones para modelizar la barra. Este código necesita una serie de parámetros iniciales para empezar a hacer las descomposiciones fotométricas sobre cada galaxia. Estos datos iniciales son tomados de imágenes de SDSS, que poseen una mayor realción señal/ruido y mejor resolución espacial para medir la estructura de las componentes de las galaxias. Estas medidas previas necesarias para el ajuste, tomadas en tres filtros (g, r e i, centrados en 4770Å, 6231Å, and 7625Å, respectivamente), en las que también se incluye el centro de cada galaxia, se dejan fijas durante todo el proceso. Las únicas variables que se dejan libres durante el ajuste son las luminosidades relativas de cada componente. Una vez modificado el código de ajuste, se ha realizado una primera prueba con una de las galaxias del set de CALIFA, concretamente con NGC0364. Los cubos de datos finales muestran que la descomposición se ha realizado correctamente, pues las tres partes han sido claramente separadas en su cubo de datos correspondiente con unos valores de brillo coherentes.

Antes de proceder a realizar la descomposición fotométrica de las galaxias reales es necesario hacer una serie de pruebas con galaxias simuladas que emulan las condiciones de las galaxias de CALIFA. Estas pruebas se han realizado con el código (escrito en IDL) create_cube, que crea una galaxia con ciertas propiedades estructurales dadas e incluye la dimensión espectral usando una librería con los espectros asociados a modelos de poblaciones simples con una edad y metalicidad dadas (librería de MILES), que se aplican a cada una de las componentes de la galaxia. Una vez generadas las galaxias, se utiliza C2D en ellas para obtener una descomposición espectro-fotométrica de bulbo, disco y barra, que a su vez se vuelven a comparar con la librería de MILES para comprobar que devuelven el mismo modelo que se les ha asignado inicialmente. En estas pruebas, además, se varían intencionadamente los parámetros fotométricos iniciales necesarios para usar C2D, simulando cómo un posible error en las medidas de estos parámetros puede inducir errores en la medida de las poblaciones estelares finales.

Una vez hecha la estimación de los posibles errores asociados a las medidas, podemos proceder a realizar la descomposición espectro-fotométrica de las galaxias barradas de CALIFA. Antes de realizar todo el proceso son necesarios algunos pasos previos. En primer lugar se suman las imágenes de todas las longitudes de onda de cada galaxia para generar una imagen de 'luz blanca'. Con estas imágenes se determina el centro de cada una de las galaxias y se observa la posible presencia de estrellas u otras galaxias que puedan contaminar el ajuste. Con la tarea 'ellipse' de IRAF creamos una máscara para cada galaxia, eliminando estas regiones del ajuste final. Además, también es necesaria la utilización de un archivo con los parámetros fotométricos iniciales de las galaxias, obtenido de los ajustes a las imágenes de SDSS en los tres filtros: g, r e i. Una vez tenemos todos estos requisitos previos procedemos a la descomposición espectro-fotométrica de las galaxias, que nos devuelve para cada una de ellas y para cada una de sus tres componentes un cubo con la información espacial y espectral combinadas y un espectro medio de esa componente, que es el que se utilizará en el siguiente paso para obtener las poblaciones estelares.

La obtención de las edades y metalicidades de las componentes galácticas se hace con el software pPXF (Penalized Pixel-Fitting, desarrollado por Cappellari & Emsellem 2004). El espectro medio de cada componente es comparado con los modelos de MILES para así obtener su edad y metalicidad típicos. Analizando los espectros de las galaxias y sus ajustes, se aprecia que hay algunos que tienen una relación señal/ruido baja y, por tanto, no es posible hacer un buen ajuste con los modelos, o que el ajuste tiene un error grande asociado. Estas galaxias, puesto que no se tiene una buena datación de su edad y metalicidad, no se tendrán en cuenta en el análisis científico final sobre las propiedades de las galaxias barradas. Por el contrario, nos serán útiles para elaborar un estudio sobre las propiedades fotométricas más óptimas que las galaxias deben tener para así conseguir el mejor ajuste posible y

la mejor relación señal/ruido en los espectros de bulbo, disco y barra. Las galaxias que presentan un buen ajuste para las tres componentes, 42 de un total de 88 que forman el set de datos, nos servirán para obtener el análisis científico de las galaxias, hecho en base a sus edades y metalicidades.

Con los resultados obtenidos se ha realizado un análisis estadístico de las propiedades de las galaxias. Se ha realizado primero un análisis técnico con todas las galaxias de la muestra de CALIFA, con los datos obtenidos de la descomposición espectro-fotométrica, analizando cuáles son las condiciones óptimas para obtener el mejor ajuste posible (que tenga el menor error asociado al hacer la comparación con los modelos). Los resultados nos dicen que las galaxias con una relación de luminosidad bulbo sobre total (B/T) menor que 0.01 o con una relación de luminosidad barra sobre total (Bar/T) menor que 0.05 son los que tienen peores ajustes, y que como más luminosa sea una componente respecto al total de la galaxia, un mayor número de galaxias con esa luminosidad tendrán buenos ajustes. Después de este primer estudio, se ha procedido a hacer un segundo utilizando solamente las galaxias que presentan un espectro menos ruidoso y que se pueden ajustar adecuadamente a los modelos de MILES. En esta sección se analizan parámetros como las edades, las metalicidades, la masa estelar o la elipticidad de las barras para averiguar si estos datos siguen tendencias claras en este conjunto de galaxias, y para comprobar si las tendencias encontradas por Méndez-Abreu et al. (2019) en galaxias con solo dos componentes (bulbo + disco) se mantienen en galaxias con un tercer elemento extra (barra). Los resultados obtenidos nos dicen que las edades de las tres componentes son bastante similares, pero que los discos normalmente son menos metálicos que las componentes internas de las galaxias analizadas. El análisis de las poblaciones estelares de las diferentes componentes parece indicar que las galaxias más masivas acretan menos gas bajo en metales (procedente del halo) que las menos masivas, una vez se han formado. Esto podría explicar la menor metalicidad en los discos de las galaxias masivas, donde las simulaciones numéricas demuestran que se acreta la mayoria del gas, con respecto a las menos masivas. También se ha podido observar que las galaxias menos masivas tienen unos discos más viejos que sus bulbos y barras, cosa que podría indicar que la barra utiliza el gas del disco para crear estrellas en el bulbo, y en sí misma, mientras que detiene la formación estelar en la región interna del disco (dentro del radio de la barra), zona que se conoce generalmente como 'desierto de formación estelar'. Además se ha encontrado que este efecto es más importante cuando la barra es más grande, lo que favorece esta interpretación.

Futuros estudios sobre las poblaciones estelares de las galaxias barradas, que tengan en cuenta la formación estelar dentro de cada componente galáctica y cómo esta se distribuye espacialmente dentro de la misma, podrían ayudar a dilucidar los efectos que tiene la barra sobre las edades y metalicidades del disco y el bulbo.

1 Introduction

1.1 Galaxy types and their properties

Galaxies are systems made of gas, stars, dust and dark matter, which are gravitationally tied and might usually have a central black hole. There are two principal types of galaxies observed, ellipticals and spirals. These galaxy types have been classified into subtypes in what is called the 'Hubble classification scheme' (Figure 1), where ellipticals are classified with the letter 'E' and a number between 0 and 7, being 0 the more roundish-shaped and 7 the more elongated ones. Spirals are classified between unbarred Sa, Sb and Sc, being Sa the more compact ones; and barred galaxies SBa, SBb and SBc, being SBa the ones with the strongest bar and being more compacted. S0 galaxies are called lenticular and they have a disk, but the spiral arms can not be seen. Spiral galaxies are flatter and bluer, because they have star formation going on in them. Otherwise, elliptical are redder and have a more roundish shape. This difference between them is related with their star formation history. In the case of the elliptical galaxies almost all the gas was consumed in the initial state of the galaxy to form stars, due to a gravitational collapse (Eggen et al. 1962) or to a merging process (Kauffmann 1996), that is the reason why most of the stars are old and red. On the other hand, spiral galaxies suffered a slower gas accretion, so the conservation of the angular momentum of the gas makes them flat (Fall & Efstathiou 1980). The surface brightness distribution of ellipticals and spirals are also different. Historically, de Vaucoulers was the first to propose a power law profile to fit their profile. This fitting was improved by Sérsic by proposing another one more general, which, depending on the value of the $R^{1/n}$ parameter, fits an exponential function valid either for bulges or elliptical galaxies with n=4 or for disks with n=1. The profile of the bar can be fitted using the Ferrers ellipsoid profile.

There are two main theories of how galaxies are formed: the 'top-down' theory claims that galaxies are formed from a huge collapse of gas. These giant structures accrete matter until they collapse and they split, becoming into the actual galaxies, both elliptical and spiral. In this scenario, galaxy clusters are formed where these giant structures intersect. The other one, the 'bottom-up' theory, maintains that at first, small galaxies were created and then they merged to create the structures that can be seen nowadays. According to this, spiral galaxies are the first to be formed and, through interaction processes, elliptical galaxies appear. The observational evidences suggest that usually isolated galaxies tend to be spiral and through interactions they become elliptical (Hopkins et al. 2009), since in dense clusters of galaxies, where galaxies have a high rate of interactions (harassment, ram pressure or tidal interactions; Boselli & Gavazzi 2014), the most common galaxies are ellipticals (giant ellipticals dominate the center of the cluster). Observations also suggest that the giant elliptical galaxies that we see in the nearby Universe were formed from a combination of both top-down and bottom-up mechanisms, with the most massive galaxies forming in the densest clusters, where both processes happened very early and quickly.

Star formation inside a galaxy can be triggered due to several processes such as inner gas collapse, minor and major mergers (mergers can trigger intense bursts of new star formation, and even make the black hole grow by the merger of the two galactic black holes or by material accreted to the galaxy center; Colpi 2014) and gas accretion from intergalactic medium. The integrated star formation rate in the Universe increases from a low initial value at $z > 6$ to a peak at $z\sim 2$, and thereafter declines (Figure 2; Madau & Dickinson 2014). The fraction of galaxy types has also changed depending on the redshift, spiral galaxies number density suffers a great increase as z decreases while irregular galaxies are the most common at the highest redshift (Abraham et al. 1996, Elmegreen et al. 2008). The structure of galaxies is thought to be usually formed inside-out. The bulges are formed first and then, after a merger, the disk or halo gas remnant contributes to form a new stellar-young disk (Hopkins et al. 2009).

Recently, several authors (Carrasco et al. 2010, Trujillo et al. 2007 and Buitrago et al. 2008) have described how the galaxy structure and size change with the redshift. The effective radii of massive galaxies is observed to be 4 times smaller at z=2 than galaxies with the same mass today. Galaxies seem to be less compact at lower z, because massive galaxies used quickly their cold gas in an efficient starburst, leaving then a less efficient heated gas to continue forming stars. Factors like mergers, galaxy formation or AGN effects can expand the effective radius of a galaxy (mergers could play the most important role in this process). Through observations, the hypothesis of the loss of density seems to be correct. Compact galaxies grow inside-out, they accrete stars far from the galactic center (van Dokkum et al. 2010). On elliptical galaxies, the inner parts become less dense while outer parts become denser. In contraposition to this, Carollo et al. (2007) found that, in spiral galaxies, half of their WFPC2+NICMOS

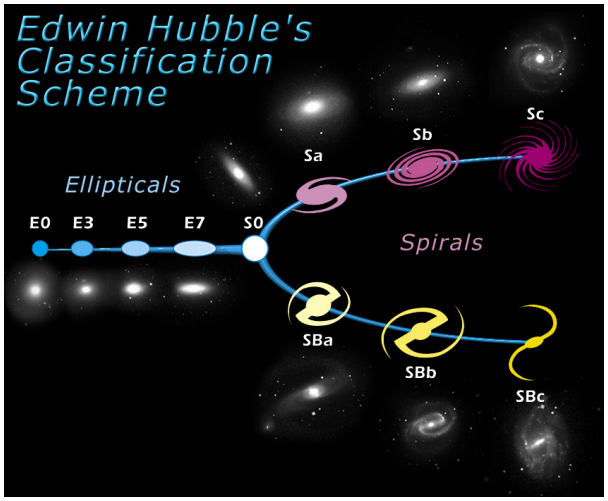

Figure 1: Image of the Hubble galaxy classification. E-type galaxies are elliptical ones, S0 are lenticular galaxies, Sa, Sb, Sc do not have a bar and SB-type contain a bar. S and SB are spiral galaxies.

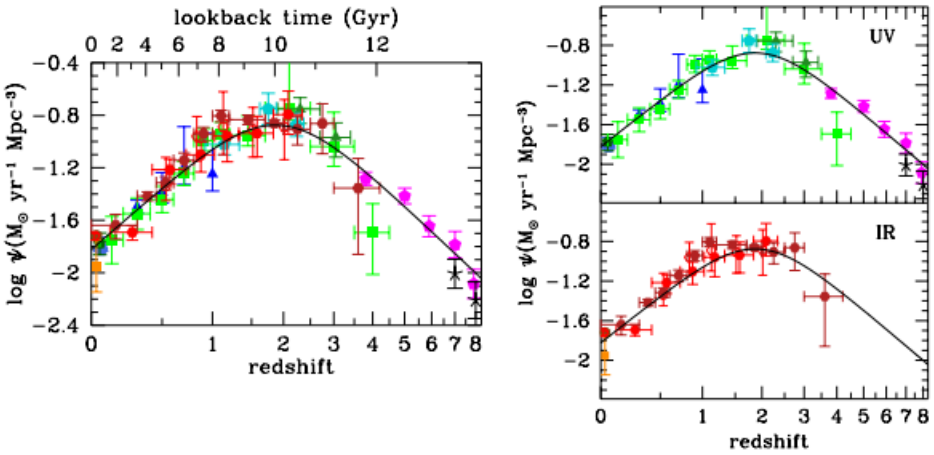

Figure 2: Figure from Madau & Dickinson (2014) representing the history of cosmic star formation from (top right panel) FUV, (bottom right panel) IR, and (left panel) FUV+IR rest-frame measurements.

sample had formed a bulge after the disk and the other half did it before. Bulges can be formed by dynamical instabilities originated internally or by a merging process, which allows them to be younger than the disk (Burnaud et al. 2007).
There are also studies (like Hathi et al. 2009) that compare the age of the bulges in early and late-type galaxies for z∼1. They found that late-type (spiral) bulges are younger than early-type (elliptical) ones at a similar redshift. This is consistent with a more long-lasting period of star formation for late-type galaxies, so their bulges have a similar stellar population to their disks.

1.2 Bars: formation, properties, effects and thickening

About two thirds of spiral galaxies have bars (Aguerri et al. 2009, Barazza et al. 2008). Bars are structures made of stars that rotate as a rigid body around the disk. This structures can be caused by gravitational instabilities in the center of the own galaxy or by gravitational perturbations caused by outer galaxies, which cause irregularities in the disk stellar distribution that leads to an elongated accumulation of gas and stars in the form of a bar.

Bars play a very important role in the structure of a galaxy, producing important changes in the disk, varying the galaxy star formation rate, stellar populations and metallicity in a time scale of a few bar rotations by redistributing angular momentum, energy, and mass (Athanassoula et al. 2013). Besides this, the bulge also notices its effects. The inflow of gas due to the bar torques could create a bulge, modify its structure and trigger AGN activity. In a lot of papers the modifying effect of the bars on galaxy properties has been discussed without getting any definitive conclusion (Vera et al. 2016, Oh et al. 2012, de Lorenzo-Cáceres et al. 2013, Gadotti 2009). The results depend on the galaxy morphology and on the length or strength of the bar. This has been found in simulations, revealing that bar strength relates with star formation activity, metallicity and pattern speed. Bars rotate around the galaxy center maintaining its shape and affecting the other structures of the galaxy (Vera et al. 2016). If they reach a cloud of molecular gas, it can increase its density inducing collapse and eventually star formation. Depending on the proximity of gas to the galactic center, the bar will treat it in a way or another. In the inner regions of the galaxy, the gas orbits with a speed higher than the bar, it passes through the bar structure and the bar gravitational pull slows down the gas and it losses angular momentum, falling into the center of the galaxy and causing star formation on the nucleus, called 'nuclear starburst'. Otherwise, if the gas is located away from the center it moves slower than the bar, so when they meet, the bar speeds up the material, pushing it out of the galaxy center.

Barred galaxies can be divided in strong-barred and weak-barred. Studies based on the images of SDSS survey (Vera et al. 2016), suggest that strong bars have lower efficiency in star formation, making the galaxy look redder. They are also more metal-rich. This is similar to the classification of elliptical and spiral galaxies: strong bars make the inflow gas quick, so the gas was quickly consumed in an early burst of star formation, while in weak bars the process lasts longer allowing a more prolonged star formation until nowadays and a bluer color. Strong bars tend to accelerate the gas processing when they become strong enough. During the process, the properties of the bar and the galaxy could change, the bar gets stronger while the galaxy gets redder and decreases its star formation rate. The shape of the galaxy is also related with the bar strength. Lenticular galaxies are found to usually have strong bars rather than weak ones. Simulations made by Khoperskov et al. (2018) show that bar quenches faster the star formation efficiency, and it does it in a short period of time (less than 1 Gyr). The faster the bar formation, the faster the star formation efficiency decreases, being also true that AGN feedback can cause the same effect by removing the gas, giving it kinematic or thermal energy or by injecting turbulence, which stabilizes the gas against fragmentation. The bar inflows the gas into the center but this gas becomes more inefficient when it comes to create stars. In the center of the galaxy, an increase of the gas amount goes together with a decrease in the star formation rate due to the gas motion. The gas loses angular momentum and falls into the galactic center, but at the same time, bar rotation increases interstellar medium turbulence that causes random gas motions. This random motions increase the dispersion of the gas, decreasing the bar star formation efficiency.

According to Sheth et al. (2008), the bar fraction is variable through time. At low redshift the bar fraction grows and the quantity of weak-barred galaxies increases. That is consistent with strong-barred galaxies being older, redder and appearing before weak ones. This is again comparable to elliptical and spiral galaxies, in which spirals appear later and are more common as the redshift decreases. It was also observed that at high redshift, the bar fraction is 0.5 if galaxies have high mass and luminosity ($\log (M_*/M_\odot) > 10.9$ and $M_V <$ -22.5) while the bar fraction drops underneath 0.2 below these values. Low mass galaxies are also susceptible to be affected by mergers, heating them up and delaying the formation of bars (Méndez-Abreu et al. 2012, 2010). This indicates that stronger bars are found in more massive and dynamically cold galaxies. According to Woo-Young et al. (2019) bars form earlier in gas-rich and cold disks, but simulations from Athanassoula et al. (2013) and observations from Masters et al. (2012) say the opposite, so this is not a clear relation. Sheth et al. (2012), analysing the galactic dynamics, also come to the conclusion that bars are not present in dispersion dominated galaxies, and that bar size grows as the disk gets colder and more massive.

Recent studies of the stellar populations in galactic bars (Seidel et al. 2016 and then Neumann et al. 2020) have shown that bars have an important age or metallicity gradient across the major axis. The gradient is much less flat in the minor axis, but is still close to zero. The gradient changes depending on the parameter considered. Studying the light profile, the gradient peaks at the center of the major axis and decreases to the edges while mass is lower at the center. This means younger stars in the center of the bar and in the extremes, and older in the edges. Besides this, younger populations tend to form a more elongated bar and older ones, a roundish bar.

In AGN galaxies the gas and angular momentum redistribution effects of the bar are more significant for bluer and less massive black hole galaxies, although AGN are more common in redder and massive galaxies, while in central star formation galaxies these effects of the bar are more important for redder galaxies. This mechanisms also increase if the size of the bar is larger. Oh et al. (2012) saw that the bar fraction is highly related with the mass of the central black hole, the higher the black hole mass the higher the bar fraction, and so it does the bar length. According to the set of galaxies they used, the fraction of galaxies with an important central star formation was the same for barred galaxies than for unbarred galaxies, unlike the AGN ones, which were much more likely to be barred. AGN galaxies are found to be more frequent in redder and more massive galaxies. Despite that, effects of the bar are higher in bluer AGN galaxies and in redder central star formation galaxies because the central mass concentration can weaken the bar structure. Even with these observational studies (SDSS), the effects of bars on AGN fueling are still not clear. Other studies like Cisternas et al. (2015), also based on observations (COSMOS survey), did not found a clear relation between AGN and bar presence/shape. AGN feedback, fueled by the gas inflow caused by the bar, consists on the AGN emmiting energy that is absorbed by the gas and inhibiting star formation. As seen in Robichaud et al. (2017), the effects of AGN feedback could be positive, by enhancing star formation, or negative, by quenching it. This overall effect is not the same if the galaxy is barred or not. For unbarred galaxies (low central gas density) the quenching near the black hole is more efficient and enhancement far from the center is less efficient, giving as a result a dominant negative feedback. On the other hand, in barred galaxies, the gas affected by the bar inflow collides with the gas ejected by the black hole and ends up in a dense ring where the star formation happens. In this case the total effect of AGN feedback is null, the positive compensates the negative so they cancel each other. AGN feedback also helps the bar grow faster and earlier by increasing instabilities. The bar grows until its maximum strength and from that moment it begins a strong oscillation superposed on a slow decay. Simulations relating the dark matter halo and the bar such as the ones from Athanassoula (2002) show that the halo and the outer disk have an important impact on the bar conditions, slowing it down. The more centrally concentrated the halo, the more efficient the slow down of the bar. In addition, the kinematic temperature is also relevant, since bars in colder disks experience a much faster lost of speed. Simulations relating the dark matter halo and bar reveal that, considering that the bar is a negative momentum perturbation in the galaxy, halos can make bars grow by taking angular momentum from them. Even so, this is not always a direct relation (the stronger the halo the stronger the bar), because it depends on the disk characteristics. If the disk is too light this mechanism will not work efficiently so bars will not be formed.
It is found on simulations that bars tend to slow down as they transfer momentum to the halo, so the stronger the bar, the faster the lost of angular momentum (Woo-Young et al. 2019). The bar gets thick until it becomes a boxy/peanut bulge.

There are three different mechanisms that thicken the bar (Sellwood & Gerhard 2020): buckling instability, vertical excitation of bar orbits by passage through the 2:1 vertical resonance (two vertical oscillation periods per orbital period in the bar frame) and a gradually increasing fraction of bar orbits trapped into this resonance. The boxy/peanut (B/P) shapes are due to star orbits above or below the disk aligned with the bar. Besides this, it has been also seen that bars can form inner bars that could have, at the same time, its own B/P shape (Méndez-Abreu et al. 2019, Ciambur et al. 2020). Inner bars were thought to have short-time life, but recent studies show that they could live Gyrs (Wozniak 2015, de Lorenzo-Cáceres et al. 2019b). This inner B/P shapes bars have even been proven observationally in a face-on galaxy (Méndez-Abreu et al. 2019).

Bar gas inflow mechanism can lead to its own destruction. If the central mass becomes large enough, it can generate orbital instabilities that end up vanishing the bar. The gas inflow affects also the bar, and this, in combination with the gravitational strength of the galactic center, thickens the bar until it combines with the nucleus (Combes 2011, Burnaud et al. 2005). This means that some of the galaxies observed today could have had a bar. The bar can also be erased due to interactions with another galaxies. After loosing the bar, the galaxy is left with a high central mass concentration and a high velocity dispersion, so the galaxy could not generate a new bar by itself. The only way this could occur is if the galaxy acquire some cold gas. This gas reduces the temperature and generates some instabilities that could allow a new bar to be formed again. Berentzen et al. (2003) described how the interactions between barred galaxies and small companions, which is quite statistically common, weaken the bars. In this simulations the barred galaxy has initially a strong bar that becomes weak or disappears after the interaction, depending on how much superficial or not the collision is rather than its duration. The effects of the interaction will not be easily appreciated after 1 Gyr.

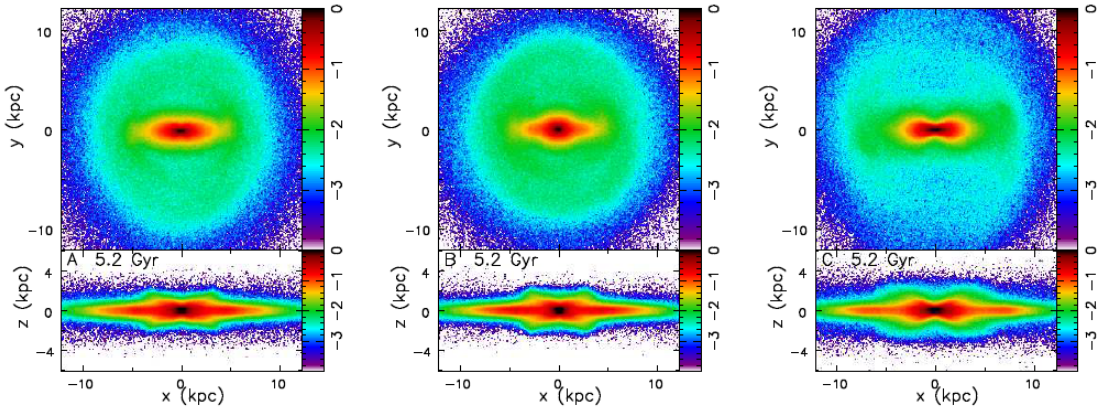

Figure 3: Example of the type of thickening of the bar in z axis, extracted from Sellwood et al. (2020). From left to right the simulated models are X-shape, boxy-shape and peanut-shape.

1.3 Aims of this Master Thesis

The study of bars is associated with a lot of uncertainty. As seen in the previous section there are several topics associated with the bar formation, their effects on the host galaxy and its relation with the galaxy formation and structure that are still unknown. Some of them such as why some galaxies have a bar or not?, when do bars form during the galaxy lifetime?, how long-lived are they? or the presence of the bar is bounded with the formation and size of AGN? To try to enlight this issues, some observational studies have used the data from Galaxy Zoo, SDSS or COSMOS surveys. The major problems with some of these data sets are the lack of image resolution of the images in order to properly distinguish the full bar component, the light contamination by external objects or the limitation in the wavelength range analysed.
The necessity for a multi-component approach to the photometric decomposition of galaxies has been demonstrated several times (Prieto et al. 2001; Gadotti 2008; Salo et al. 2015). Specifically, including the bar component has been proved to be critical in order to recover accurate bulge parameters (Aguerri et al. 2005; Laurikainen et al. 2005). Several studies have shown that both the Sérsic index (n) and the bulge to total luminosity ratio (B/T) can be artificially increased if the bar is not properly fitted (Gadotti 2009; Weinzirl et al. 2009; Méndez-Abreu et al. 2014)

There is a need of having bar spectra free from bulge and disk light contamination to do a detailed study of their stellar populations, and how these relate with bar photometric properties, to answer the questions previously formulated at the beginning of the section. To perform such a detailed study of the bar properties, the best data that can be obtained is by using Integral Field Spectroscopy (IFS), which allows to obtain spatially resolved spectral data. For this purpose the data from the Calar Alto Legacy Integral Field Area (CALIFA) survey is used. This work presents a novel analysis of barred galaxies using IFS, allowing to not only having a well resolved photometric decomposed image of the bar, but obtaining its spatially resolved spectra. This analysis using a new method to perform spectro-photometric bar decompositions, obtained also for the bulge and disk, will allow to get their populations, to compare them, to do statistics with the set of 88 CALIFA barred galaxies used and to try to understand the history formation of barred galaxies and how the components of these galaxies affect each other.

The aim of this work is to continue and to extend the work of Méndez-Abreu et al. (2019) (explained in Section 3.1) by adding the bar structure to the spectro-photometric decomposition of galaxies (Section 3.2). The C2D code has been used over two component galaxies (bulge+disk) with accurate results. Adding a third component to the spectro-photometric decomposition gives a more complex process to be tested, but also opens a wide range of possibilities by studying the bar component.
The addition of a bar component to the spectro-photometric decompositions requires, in addition, some tests with mock galaxies (Section 4) to ensure the good behaviour of the code and to research how the brightness, the age and the metallicity of each of the three components can modify the errors of the decomposition and could lead to a not proper obtaining of the age and metallicity.

2 The CALIFA dataset

2.1 Introduction to CALIFA

The Calar Alto Legacy Integral Field Area (CALIFA) is one of the largest integral field spectroscopy surveys. CALIFA observations started in June 2010. About 20 galaxies were observed per month from a total observation time of 210 dark nights at CAHA over 3 years. Its dataset contains 667 galaxies (1576 datacubes) in the Local Universe (0.005<z<0.03), which are diameter selected to fit into the field-of-view of CALIFA (1'x1'). All the data from this survey is free to public access. There is a Main Sample with the characteristics just enunciated, but there is also a Extension Sample that covers several types of galaxies that are rare and therefore, not numerous or absent in the CALIFA Main Sample. The most abundant galaxies in DR3 sample are Sb and Sbc type galaxies.

CALIFA uses the PPAK Integral Field Unit (IFU), mounted at the Calar Alto 3.5m telescope, with a hexagonal field-of-view of 74"x64". The optical wavelength range is 3700 to 7000 Å. It has tree overlapping setups with different resolutions: a low-resolution V500 setup covering the wavelength range 3745–7500 Å with a spectral resolution of 6.0 Å (FWHM), for 646 galaxies, a medium-resolution V1200 setup covering the range 3650–4840 Å with a spectral resolution of 2.3 Å (FWHM), for 484 galaxies, and a third one combination of the previous two, called COMBO, with a spectral resolution of 6.0 Å and a wavelength range between 3700-7500 Å, for 446 galaxies. The first setup is designed to study stellar populations and the properties of the ionized gas, while the second setup is more adapted to measure precisely stellar and ionized gas kinematics kinematics. Exposures for V500 grating last 900 seconds per pointing, complemented by the 3 exposures of 600 seconds taken by V1200 grating. The CCD used is a 4k x 4k E2V detector. Datacubes reach a 3 σ limiting surface brightness depth of $\sim$ 23.0 mag/arcsec^2 for the V500 grating data and $\sim$ 22.8 mag/arcsec^2 for V1200. The measured spectral resolution is $\sim$85 km/s for V1200 and $\sim$ 150 km/s for V500. The PSF of the datacubes has a mean value of 2.5". Around 60 % of the CALIFA galaxies have disk components (Sánchez et al. 2012), including irregulars and interacting galaxies, which have active star formation. Over 200 galaxies are, then, early type. CALIFA has an accurate spatial sampling, with a typical spatial resolution of $\sim$ 1 kpc. The reduction of the data is performed by a pipeline without human intervention that provides scientific frames and also a set of quality control measurements to estimate the accuracy of the data.

The main advantages of this survey compared to its predecessors are: large number of objects (so statistical analysis can be performed), a broad coverage of galaxy subtypes and environmental conditions, allowing universal conclusions, and the homogeneity of the data acquisition. The principal measures CALIFA was designed for are: gas ionization mechanisms, ionized oxygen and nitrogen abundances, stellar population properties (age, metallicity and mass-to-light ratios) and kinematics of galactic gas and stars (Figure 4). The scientific goals of the survey are to characterize the properties of the ionized gas, to determine the current SFR, metallicity and the relative importance of AGN activity in the overall evolution of galaxies. In summary, to increase our knowledge of the baryonic physics of galaxy evolution.

From the CALIFA absorption line spectra, it can be obtained information on ages (and therefore mass-to-light ratios) and metallicities of the stellar population. CALIFA emission line spectra gives information about dust attenuation, star formation rates, excitation mechanisms and ionization parameters, gas metallicities and electron densities. In addition, global information from CALIFA allows to not only classify galaxies through their kinematics, but to build rotation curves and dispersion profiles, as well as detailed mass models for a large sample of galaxies. Some of the science goals that have been addressed thanks to this dataset are: to explore the galactocentric radial gradient of the oxygen abundance (Sánchez et al. 2012b), to confirm that up to $\sim$2 disk effective radius there is a negative gradient of the oxygen abundance in all the analyzed spiral galaxies; developing of new techniques to understand star formation histories (SFH) of galaxies (Cid Fernandes et al. 2013, 2014); finding that mass-assembly happens inside-out (Pérez et al. 2013) and that age and metallicity gradients of spirals are not significantly altered by bars (Sánchez-Blázquez et al. 2014); studying kinematics of galaxies for all types of morphologies, including kinematics of ionized gas (García-Lorenzo et al. 2015) and the effects of bars in galactic kinematics (Barrera-Ballesteros et al. 2014) or angular momentum of galaxies (Falcón-Barroso et al. 2015).

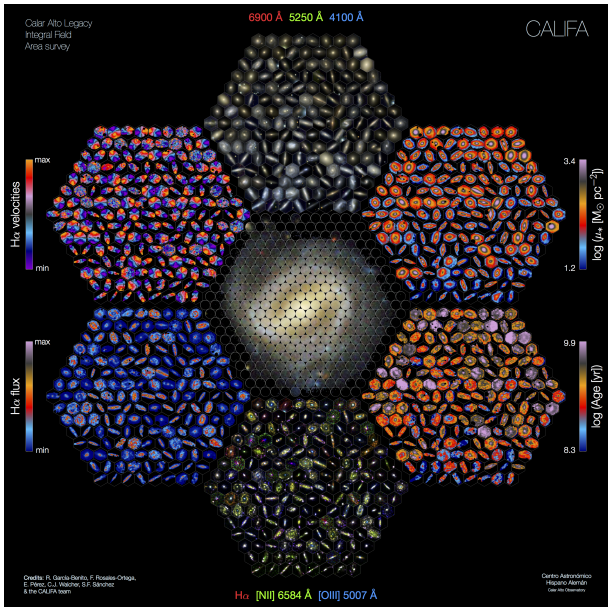

Figure 4: Logo of the Calar Alto Legacy Integral Field Area (CALIFA) survey. The measures obtained from the CALIFA datacube have a FoV of 1'x1', the wavelength range is 3700-7000Å . and they can be used to obtain the gas and ionization abundances, stellar population properties and kinematics of the galaxies.

2.2 CALIFA photometric decompositions

The multi-component photometric decompositions of the CALIFA DR3 sample were presented in Mendez-Abreu et al. (2017). They presented a detailed analysis of the main structures present in the galaxies including: bulges, discs, and bars, assuming flat cosmology (Ω_m=0.3, Ω_Λ=0.7 and a Hubble constant H_0= 70 km/s/Mpc). To do the photometric decomposition, one of the previous steps is to check the conditions of the galaxy image. From the total DR3 sample of 667 galaxies, only 404 were finally used. The galaxies that are paired and interacting (57) or with a distorted morphology were not suitable for photometric decomposition. Besides this, characterization of structural properties in galaxies with an excessive inclination is not possible, so galaxies close to edge-on configuration (i > 70^o) are also discarded (183). After this, the images are examined looking for bright stars that contaminate the galaxy image and mask them, but some of them were too invasive so 5 more galaxies were discarded

In order to perform the 2D photometric decomposition, the GASP2D code (Méndez-Abreu et al. 2008, 2014) is used. GASP2D uses a Leverberg-Marquard algorithm to fit the 2D surface brightness distribution (SBD) of galaxies with a set of model components. GASP2D simultaneously fits the galaxy structures: nuclear point source (NPS), bulge, bar, and disk (including breaks). Each isophote of each component is a perfect ellipse centred on (x_0, y_0) with constant position angle (PA) and constant ellipticity (ϵ = 1 - q), where q is the minor-to-major axis ratio of the ellipse. The geometric parameters (PA, ϵ) are independent for each component. The isophotal radius r follows the expression:

$$r = \left[(-(x-x_0)sin(PA) + (y-y_0)cos(PA))^2 + (-(x-x_0)cos(PA) - (y-y_0)sin(PA))^2/q^2\right]^{1/2} \quad (1)$$

The SBD of the bulge component is a Sérsic profile (Sérsic 1968), also known as the $r^{1/n}$ law:

$$I_b(r_b) = I_e \cdot 10^{-b_n\left[(\frac{r_b}{r_e})^{1/n}-1\right]} \quad (2)$$

where r_b is the radius measured in the Cartesian coordinates describing the reference system of the bulge. r_e, I_e, and n are the effective (or half-light) radius, the surface brightness at r_e, and the Sérsic index describing the curvature of the SBD, respectively, and b_n = 2n - 0.3271 (Graham & Driver 2005).

The NPS replies the point spread function (PSF) of CALIFA images using a Moffat function. Including a NPS to properly derive the bulge parameters when nuclear stellar clusters (NSC) (Balcells et al. 2007) or AGN (Benítez et al. 2013) are present has been proven necessary in several works. NPS models an unresolved bulge with a size comparable to the image PSF. The NPS parameterisation is given by:

$$I_{NPS}(r_{NPS}) = I_{NPS}\left(1 + \left(\frac{r_{NPS}}{\alpha}\right)^2\right)^{-\beta} \tag{3}$$

α and β define the profile shape and relate to the FHWM such as FWHM=$2\alpha\sqrt{2^{1/\beta}-1}$.

The SBD of a galactic disk is usually described with an exponential profile. However, nowadays it is commonly accepted that galaxy discs can be classified into three general categories (Erwin et al. 2005; Pohlen & Trujillo 2006): (i) profiles that follow a single exponential profile along the whole optical extent of the galaxies, (ii) profiles that present a double exponential law with a down-bending beyond the so-called break radius, and (iii) profiles that exhibit an up-bending in the outer parts of the discs. To account for these possibilities the following parameterisation is adopted:

$$I_d(r_d) = I_0 \cdot \left[e^{-\frac{r_d}{h}}\theta + e^{-\frac{r_{break}(h_{out}-h)}{h_{out}\cdot h}} \cdot e^{-\frac{r_d}{h_{out}}}(1-\theta)\right] \tag{4}$$

θ has value 0 for $r_d > r_{break}$ and value 1 for $r_d < r_{break}$ and r_d is the radius measured in the Cartesian coordinates describing the reference system of the disc. I_0, h, h_{out}, and r_{break} are the central surface brightness, inner scale-length, outer scalelength and break radius of the disc, respectively.

The projected surface density of a three-dimensional Ferrers ellipsoid (Ferrers 1877, Aguerri et al. 2009) describes the SBD of the bar component:

$$I_{bar}(r_{bar}) = I_{0bar}\left[1 - \left(\frac{r_{bar}}{a_{bar}}\right)^2\right]^{n_{bar}+0.5} \tag{5}$$

where r_{bar} is the radius measured in the Cartesian coordinates describing the reference system of the bar. I_{0bar}, a_{bar}, and n_{bar} are the central surface brightness, length, and shape of the bar, respectively. n_{bar} has a high degeneracy, so it is fixed to n_{bar}=2.

CALIFA datacubes do not have enough spatial resolution to carry out an accurate photometric decomposition, and since the CALIFA survey is designed based on the SDSS survey, it was decided to use the better spatial resolution SDSS imaging (in three bands) to perform the decomposition. SDSS data is used to set the initial input photometric parameters. They were derived independently for the three SDSS bands (g, r, and i). Besides this, some input files required are: a sky-subtracted image of the galaxy, a mask to avoid foreground stars, background galaxies and other features that could contaminate the galaxy image, and the radial profiles of ellipticity, position angle, and surface brightness. The sky-subtracted image is obtained by averaging a region with a flat surface brightness at a radius where neither the galaxy nor other sources are affecting the flux. The masks are created using SExtractor and other tools as the task 'ellipse' from IRAF. The isophotal profiles are derived using the sky-subtracted images. 'ellipse' is run again allowing the isophotes to change the values of ϵ and PA to follow the galaxy morphology. The masks created during the sky subtraction process were used to derive these 1D profiles needed.

SDSS PSF is modeled with a Moffat function (Eq. 3). For each galaxy image, a set of at least five non-saturated stars were fitted with a Moffat function using the IRAF task 'imexam'. GASP2D uses the measured PSF as kernel to be convolved with the model galaxy image before computing the χ^2. This process is repeated in each iteration of the Levenberg-Marquardt minimisation process so that the final best-fit parameters are seeing-corrected.

Small bulges with sizes comparable to the SDSS PSF can lead to erroneous fits, leading to extreme values of the Sérsic index (n > 7). These galaxies are fitted using a NPS instead of the Sérsic function for the bulge. A bulge and a NPS would never be fitted simultaneously in the same galaxy, and galaxies better represented by a NPS should not be understood as necessarily hosting a nuclear star cluster or AGN.

To perform the photometric decomposition of a spiral galaxy, the starting point is a two-component bulge+disk fit. After this, or from the start if its presence is readily apparent in the galaxy image, the addition of a bar component is checked. If the bar is not obvious in the galaxy image, both the bulge+disk and bulge+disc+bar fittings are performed. Then an analysis of the residuals, ϵ and PA is made to confirm the existence of the bar. The presence of a broken disk is also performed.

To provide an error associated with the structural parameters some mock galaxies were simulated. Mock galaxies are placed at a distance of 67 Mpc, that corresponds to the median value of our the real sample. Galaxies are convolved with the mean PSF of the i band of SDSS images to reproduce the typical spatial resolution. In addition, some extra adjustments to emulate real SDSS images are applied, like the pixel scale (0.396 arcsec/px), the typical values of the CCD gain (4.86 e^-/ADU) and the read-out noise (5.76 e^-). The mock galaxies are then fitted using GASP2D. The comparison between the input and output values of the fitted parameters is used to compute the errors.

2.3 The set of barred galaxies used

The galaxy sample used in this work comprises all the barred galaxies in the CALIFA dataset that have a fitted bulge, bar and disk. Additional criteria like to not having truncated disks or not hosting nuclear point sources are also considered. This leaves a finals set of 88 barred CALIFA galaxies that will be used for the spectro-photometric decomposition (see Figure 5).

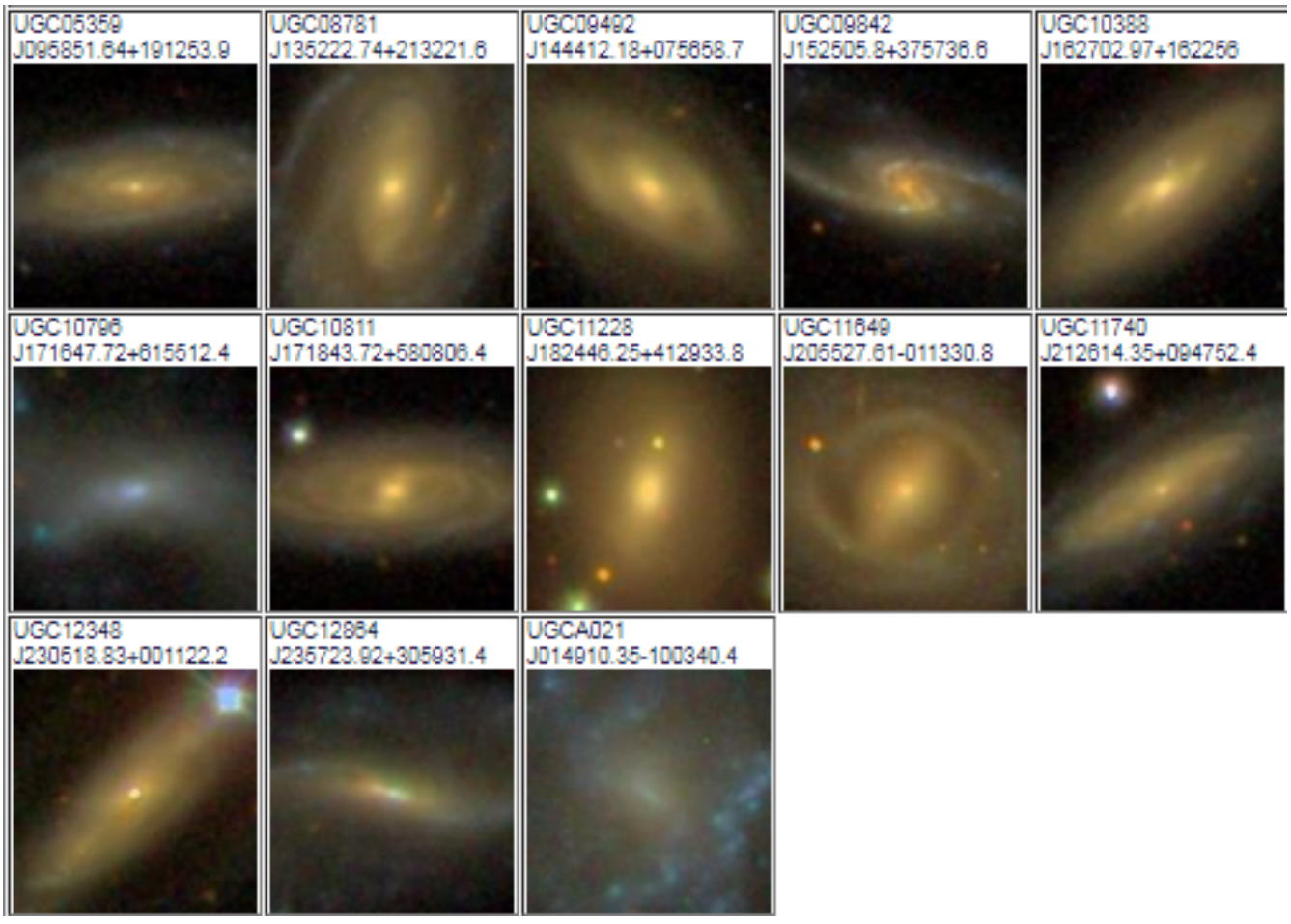

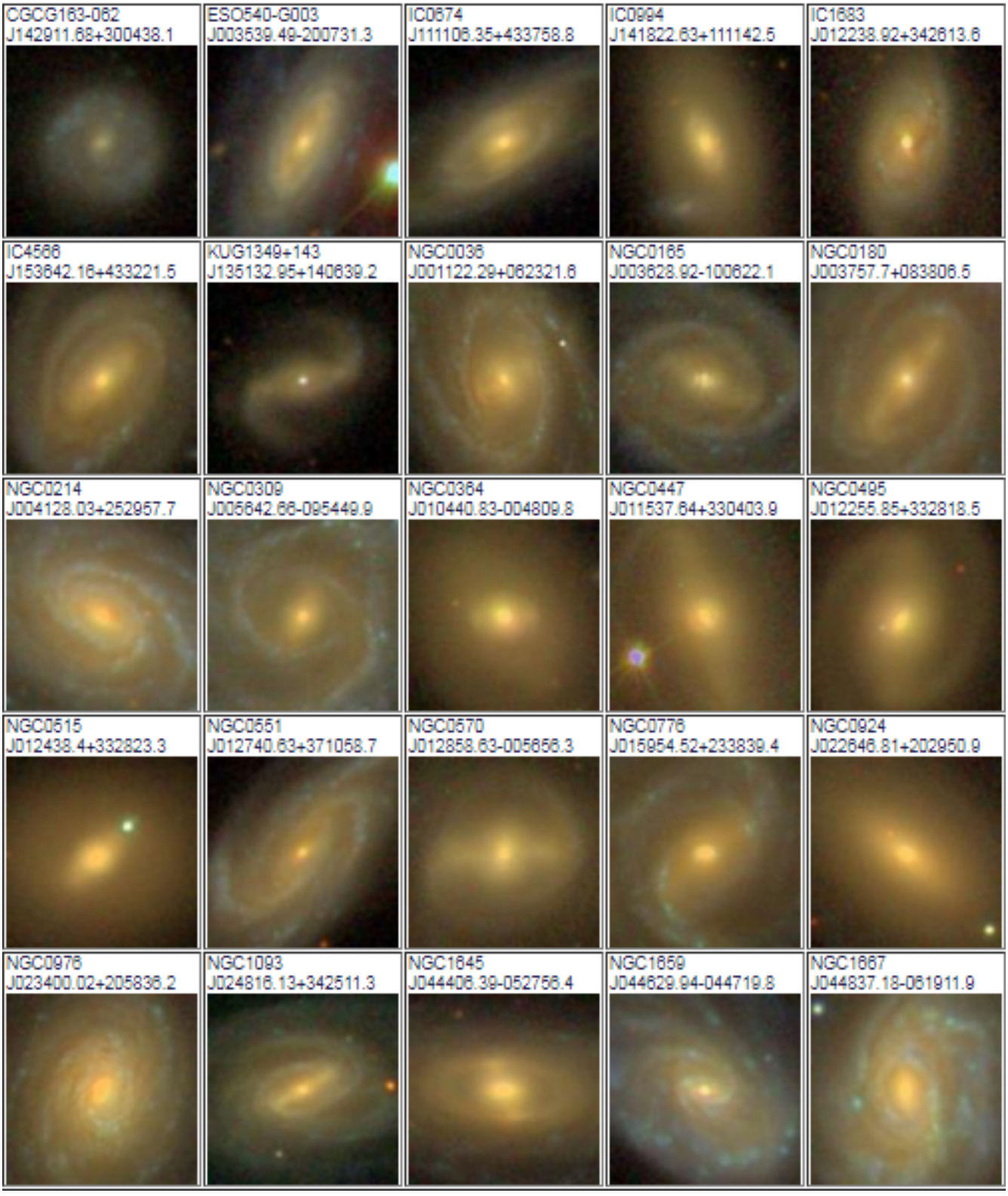
CGCG163-062
J142911.68+300438.1
ESO540-G003
J003539.49-200731.3
IC0674
J111106.35+433758.8
IC0994
J141822.63+111142.5
IC1683
J012238.92+342613.6
IC4566
J153642.16+433221.5
KUG1349+143
J135132.95+140639.2
NGC0036
J001122.29+062321.6
NGC0165
J003628.92-100622.1
NGC0180
J003757.7+083806.5
NGC0214
J004128.03+252957.7
NGC0309
J005642.66-095449.9
NGC0364
J010440.83-004809.8
NGC0447
J011537.64+330403.9
NGC0495
J012255.85+332818.5
NGC0515
J012438.4+332823.3
NGC0551
J012740.63+371058.7
NGC0570
J012858.63-005656.3
NGC0776
J015954.52+233839.4
NGC0924
J022646.81+202950.9
NGC0976
J023400.02+205836.2
NGC1093
J024816.13+342511.3
NGC1645
J044406.39-052756.4
NGC1659
J044629.94-044719.8
NGC1667
J044837.18-061911.9

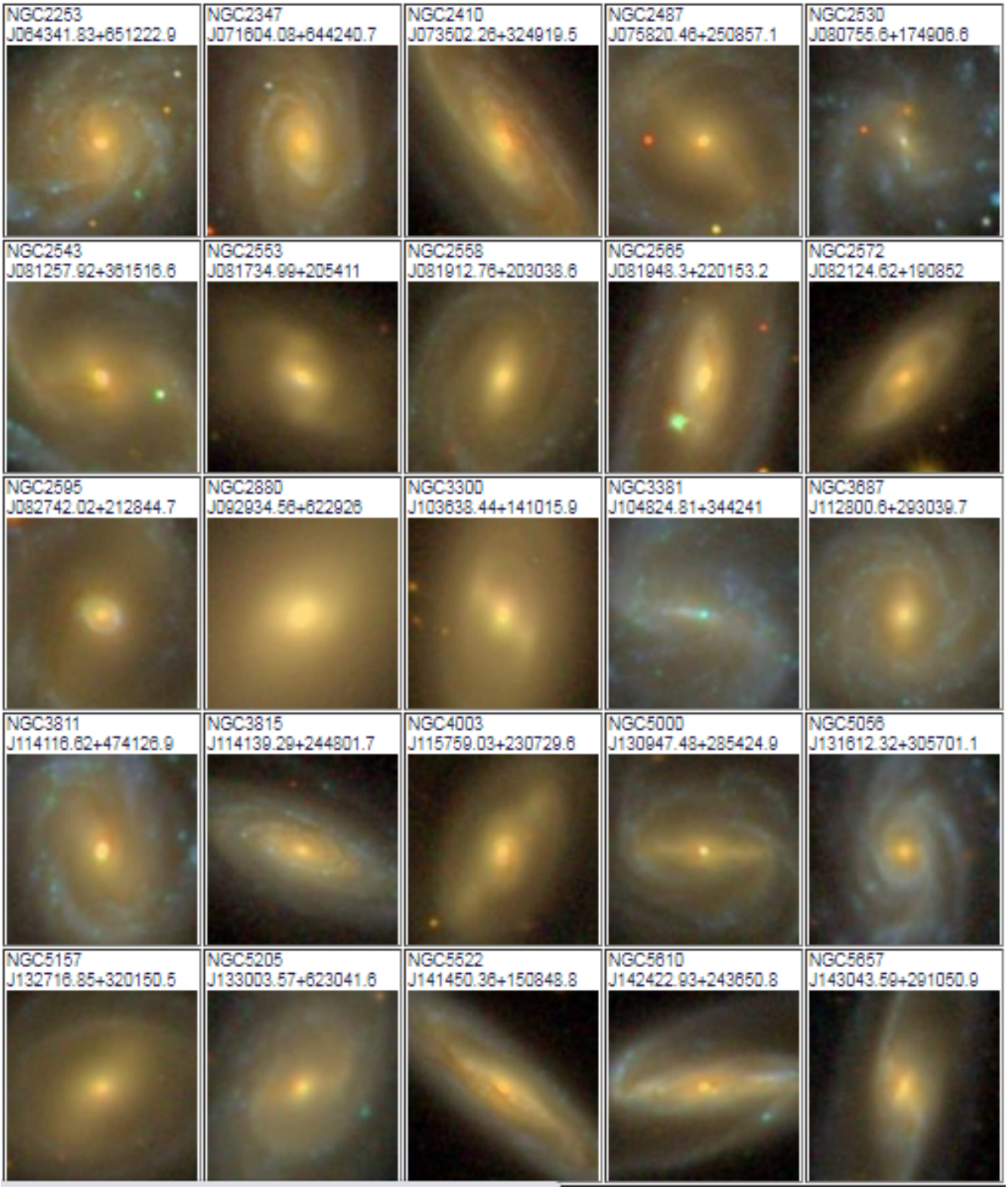
NGC2253
J064341.83+651222.9
NGC2347
J071604.08+644240.7
NGC2410
J073502.26+324919.5
NGC2487
J075820.46+250857.1
NGC2530
J080755.6+174906.6
NGC2543
J081257.92+361516.6
NGC2553
J081734.99+205411
NGC2558
J081912.76+203038.6
NGC2565
J081948.3+220153.2
NGC2572
J082124.62+190852
NGC2595
J082742.02+212844.7
NGC2880
J092934.56+622926
NGC3300
J103638.44+141015.9
NGC3381
J104824.81+344241
NGC3687
J112800.6+293039.7
NGC3811
J114116.62+474126.9
NGC3815
J114139.29+244801.7
NGC4003
J115759.03+230729.6
NGC5000
J130947.48+285424.9
NGC5056
J131612.32+305701.1
NGC5157
J132716.85+320150.5
NGC5205
J133003.57+623041.6
NGC5522
J141450.36+150848.8
NGC5610
J142422.93+243650.8
NGC5657
J143043.59+291050.9

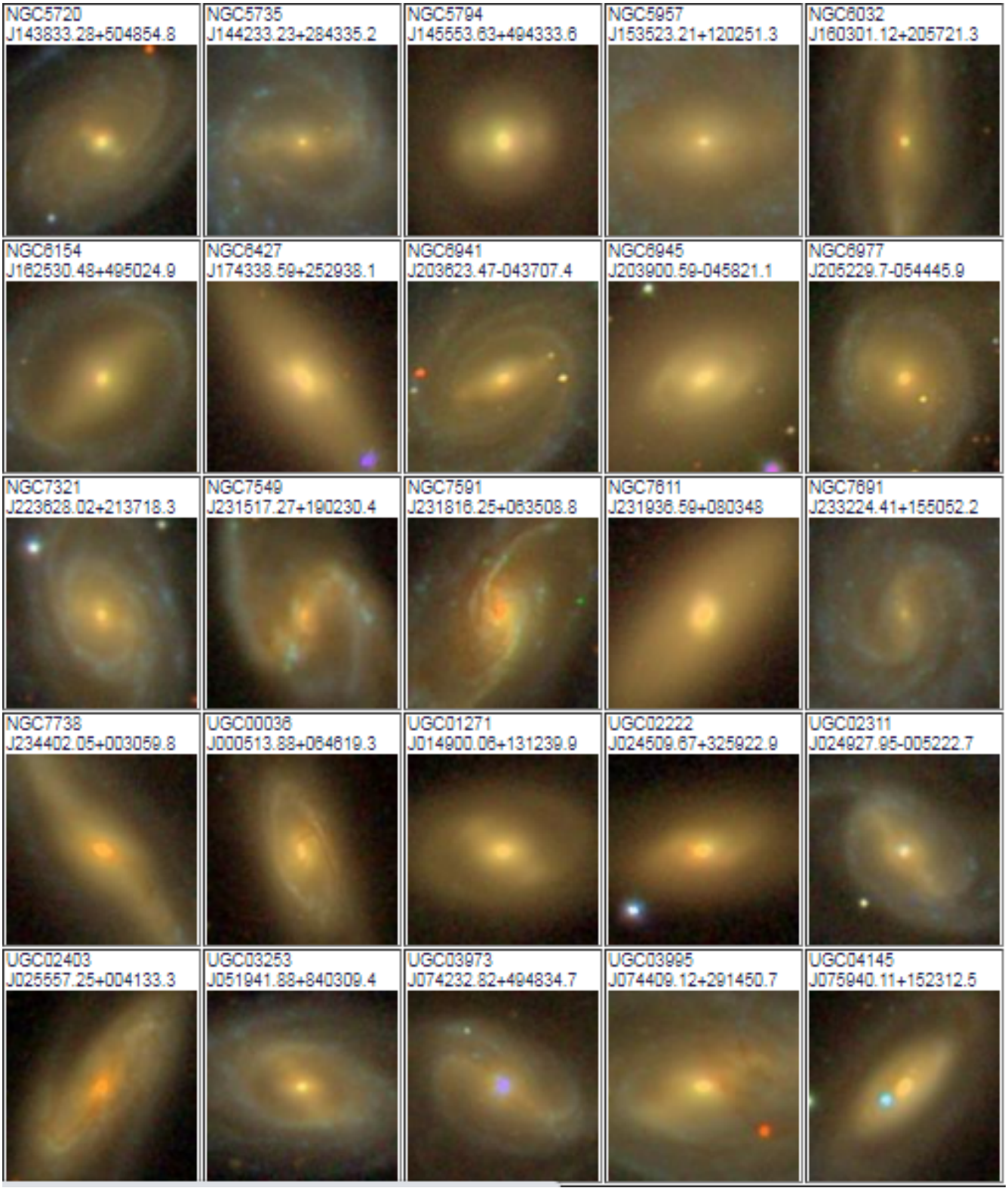

Figure 5: Images of the 88 barred galaxies selected for this work from the SDSS catalogue.

3 Adding a bar structure to spectro-photometric decompositions

3.1 C2D Description

In Méndez-Abreu et al. (2019), the C2D algorithm to perform spectro-photometric multi-component decompositions of integral field spectroscopy (IFS) datacubes was introduced. This code is used to separate the spectral information of multiple components in an IFS datacube using 2D photometric decompositions of their SBD (Figure 6). C2D provides both a characteristic 1D spectra and a datacube with all the spatial information for each component included in the fit (bulge and disk). This algorithm is an extension of the photometric decompositions that have been done in the broadband images, by performing a fit of each wavelength image of the IFU datacubes.

The main engine of C2D is to perform 2D photometric decompositions of large a set of images. This task is carried out in C2D by the GASP2D algorithm (Méndez-Abreu et al. 2008, 2014). The code fits a set of analytical models to the galaxy (see Section 2). The minimisation is performed using a Levenberg-Marquardt algorithm and the galaxy model is convolved with the data point spread function (PSF) at each iteration before comparing with the real observations. The equations 2, 4 and 5 are used to model the bulge, disk and bar, respectively. In the initial C2D code only bulge and disk were used, but since the aim of this Master thesis is to analyse a set of barred galaxies, the bar part has been added in the v2.0 version (next Section). The three components are built into three independent reference frames centred at the galaxy centre (x_0, y_0), but with different axis ratios ($(b/a)_b$, $(b/a)_d$, $(b/a)_{bar}$) and position angles (PA_b, PA_d, PA_{bar}).

To perform a photometric decomposition of the CALIFA datacubes, some free parameters need to be fitted. This 11 free parameters are five for the bulge component: (μ_e, r_e, n_b, $(b/a)_b$ and PA_b), four for the disk (μ_0, h, $(b/a)_d$ and PA_d) and the galaxy center (x_0, y_0). Then some extra parameters for the bar will be added. If these parameters are left free to fit, the computing capacity needed would be too much. Besides this, the S/N and spatial resolution of the CALIFA images could induce some extra problems when doing the photometric decomposition. For these reasons, a strategy to ensure the best measuring possible and to reduce the computing capacity was designed. It consists on using SDSS multi-band photometric decompositions of the CALIFA sample to have the initial parameters values (Méndez-Abreu et al. 2017), given that SDSS images have enough S/N and spatial resolution (2 times better PSF). The SDSS bands used are g, r and i, with central wavelength at 4770 Å, 6231 Å, and 7625 Å, respectively. These three filters are used because the characteristics of the parameters vary depending on the wavelength. The variation of the photometric parameters of SDSS was tested for different approximations, concluding that the linear fit was the best, so a linear fit of the three values of each parameter is performed. In the case of the galactic center, all the wavelength images are integrated and the most bright central pixel from the galaxy is designed as galactic center (with sub-pixel precision). Then, when executing C2D to create the datacubes, all the free parameters are fixed according to the value obtained from the SDSS data, except for the intensities of the bulge and disk (μ_e and μ_0), that are left free to vary during the fit.

When applying C2D to CALIFA datacubes, the first step is to collapse them into narrow-band-like images to increase the S/N. The CALIFA datacubes are collapsed into 10 different narrow band images of $\sim$ 375 Å each one. Then GASP2D performs the photometric decomposition over them. As said before, the structural parameters of the bulge, disk and bar are fixed to the linearly interpolated values in the corresponding wavelength bins. The intensities are the only ones to be fitted. The best fitted intensities are then linearly interpolated to the full wavelength grid to be used as initial conditions for the final fit. The next step is to perform the photometric decomposition to each quasi-monochromatic image of the datacube. The values for each parameter derived from the linear interpolation of the narrow band images will be used as initial conditions. Then, the fit is done with all parameters allowed to vary. In this case, the structural parameters are kept fixed and only the intensities are free to vary.

The analysis of the CALIFA datacubes provides a characteristic spectra for the three components. C2D also creates a datacube with spatial and spectral information for each component. The photometry performed at each CALIFA datacube when fitting the intensities extracts the luminosity contribution of bulge (B/T) disk (D/T) and bar (Bar/T) to the total galaxy luminosity for each spaxel. Each fraction is then multiplied by the observed CALIFA datacube in that spaxel and wavelength.

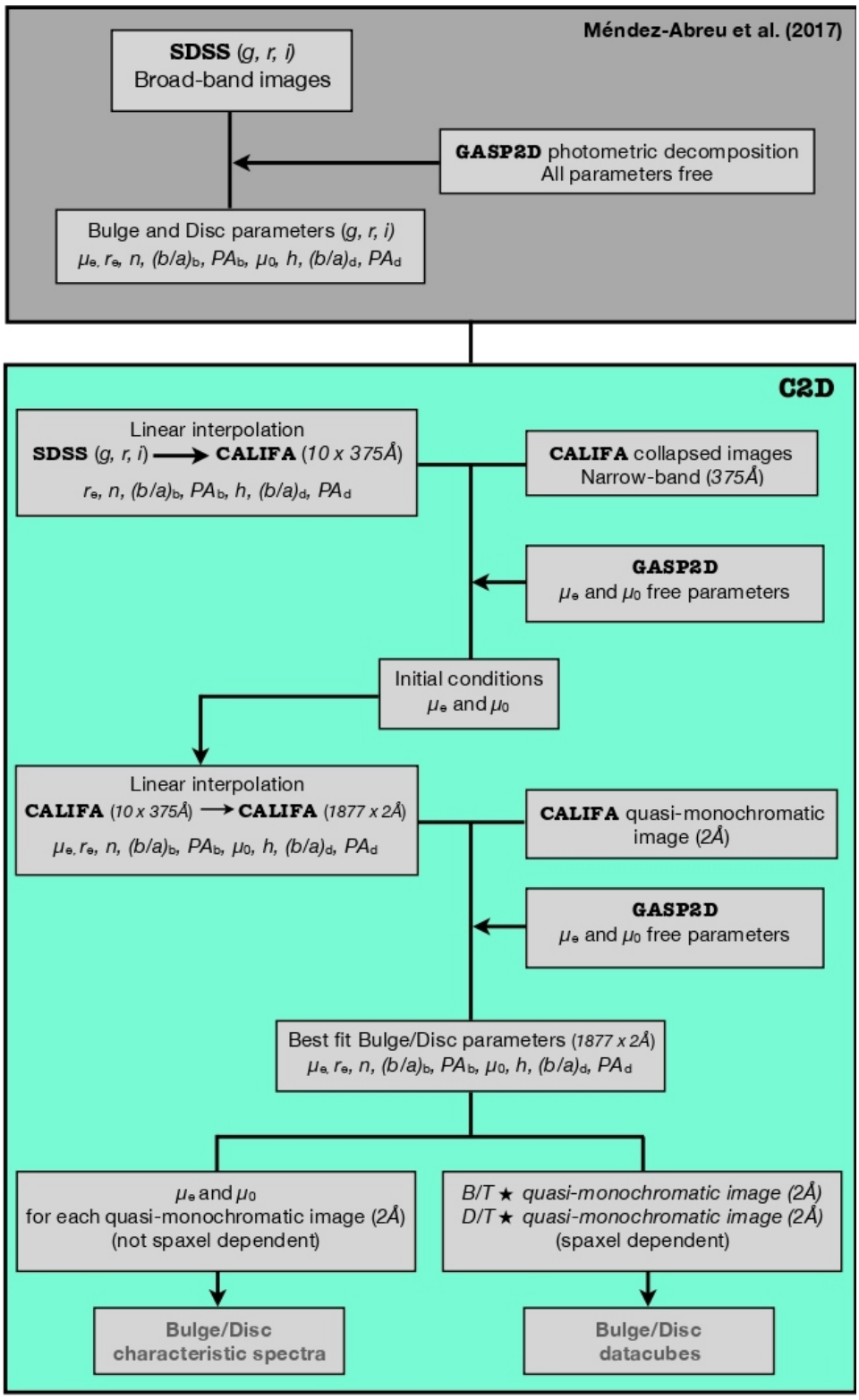

Figure 6: Schematic of the C2D code. The upper panel describes the 2D photometric decomposition carried out using SDSS images, and used as an input to C2D (Méndez-Abreu et al. 2017). The lower panel shows the different steps followed by C2D to provide the two outputs: the characteristic 1D bulge/disk spectra and the 2D datacubes.

3.2 C2D v2.0

The aim of this project is to add a bar component to the C2D code to process barred galaxies. For this purpose the algorithm of GASP2D was already set previously, so the main changes were done in C2D.

The projected surface density of a three-dimensional Ferrers ellipsoid is used to describe the surface brightness distribution of the bar component, as seen in Méndez-Abreu et al. (2017) and section 3.2 (equation 5), but applying a restriction condition:

$$I_{bar}(r_{bar}) = \begin{cases} I_{0bar}\left[1-\left(\frac{r_{bar}}{a_{bar}}\right)^2\right]^{n_{bar}+0.5} & r_{bar} \leq a_{bar} \\ \\ 0 & r_{bar} \geq a_{bar} \end{cases} \tag{6}$$

The default value for n_{bar} used is $n_{bar} = 2$ (Laurikainen et al. 2005).

The free parameters, now including the bar ones: μ_{0bar}, r_{bar}, n_{bar}, $(b/a)_{bar}$, and PA_{bar}, are still fixed with the interpolation of the values obtained from the SDSS photometric decomposition, leaving the intensities of the three components (μ_e, μ_0 and μ_{0bar}) free to vary. GASP2D, through these expressions, makes the photometric decomposition of the input datacube into bulge, disk and bar. The luminosity contribution of each component (B/T, D/T and Bar/T) compared with the total for each spaxel is also obtained. The fractions are then multiplied by the CALIFA datacube for every spaxel and its wavelengths, obtaining a final datacube image for the three components. C2D provides also the characteristic spectra for the bulge, disk and bar components.

4 Mock galaxy simulations

4.1 Adding a bar structure to create mock galaxies

In order to test the correct behavior of the C2D code some tests were performed. These tests consist on generating mock galaxies with different conditions and run C2D on them to ensure the input parameters assigned equal the final results obtained from C2D. For this purpose, a code already available from generating galaxy datacubes, called create_cube.pro, has also been modified to include the bar component. This code takes some input photometric parameters, which are μ_e, r_e, n, B/T and the inclination angle of the bulge; μ_0, h, D/T and the inclination of the disk and μ_{0bar}, r_{bar}, n_{bar}, Bar/T and the inclination angle of the bar.

After setting the galaxies parameters, the PSF is fixed to the same value that CALIFA images have. The next step is to give each component a spectra with the age and metallicity information desired. With all these initial conditions, the datacubes are created specifically configured to have the same dimensions as the CALIFA ones. The magnitude of the total galaxy is distributed in the different components according to the equations below:

$$L_{tot} = 2 \cdot \pi \cdot I_e \cdot r_e^2 \cdot n \cdot \frac{exp(b_n) \cdot \gamma(2n) \cdot (b/a)_b}{b_n^{2n}} \tag{7}$$

The total luminosity is then used to calculate each component model: L_{bulge} = B/T · L_{total}, L_{disk} = D/T · L_{total} and L_{bar} = Bar/T· L_{total}. Then, the effective intensities of each component are calculated using:

$$I_e = \frac{L_{bulge}}{2 \cdot \pi \cdot r_e^2 \cdot n \cdot \frac{exp(b_n) \cdot \gamma(2n) \cdot (b/a)b}{b_n^{2n}}} \tag{8}$$

$$I_0 = \frac{L_{disk}}{2 \cdot \pi \cdot h^2 \cdot (b/a)d} \tag{9}$$

$$I_{0,bar} = \frac{L_{disk} \cdot \gamma(9/2)}{\pi \cdot r_{bar}^2 \cdot \gamma(5/2) \cdot (b/a)_{bar}} \tag{10}$$

where $(b/a)_i$ are obtained with the cosine of the inclination angles of each component.
The final model is obtained with the expressions of the section 2.1:

$$I_{bulge} = I_e \cdot exp(-bn \cdot ((r_b/r_e)^{1/n} - 1D)) \tag{11}$$

$$I_{disk} = I_0 \cdot exp(-r_d/h) \tag{12}$$

$$I_{bar} = I_{0,bar} \cdot (1 - (r_{bar}/a_{bar}^2)^{n_{bar}+0.5}) \tag{13}$$

The final models are then resampled to the dimensions of the CALIFA galaxies and a final datacube for each one of them is obtained, which will be used to test the accuracy and behavior of C2D. The final datacube can also be added a desired value for the S/N. To include the spectral part, the MILES library (Sánchez-Blázquez et al. 2006, Falcón-Barroso et al. 2011) is used. This library contains single stellar population (SSP) models based on an empirical library. The mock galaxies are generated using the spectral dispersion of CALIFA. For simplicity only one SSP is used for each component. When the mock galaxies are generated, C2D is run over them exactly in the same way as if they were CALIFA galaxies to obtain each component datacube. The final step of all this process, and as part of the work of this thesis, is to add the bar part in the code create_errors. This code takes each one of the three datacubes the code C2D has generated for bulge, disk and bar and compares it to the whole set of MILES templates to obtain their age and metallicity. Depending on how the processes modify the spectra between the initial templates and the final images the code create_errors receives, the final predictions will be more or less similar to the input made in create_cube.pro.

This code, called create_errors, reads the MILES models and extracts their properties. Then takes from each C2D output datacube the mean spatial values of each galaxy component to generate a final spectra. The code calculates the χ^2 values between each component spectrum and all the MILES templates spectra and gives a final output with the values of the age and metallicity with the lowest χ^2. This output files will be used in the next section to elaborate the plots to understand the accuracy and robustness of C2D.

4.2 Decomposing mock galaxies

To test if C2D is actually decomposing the datacubes satisfactorily for all the possible configurations the CALIFA galaxies could have, a diverse set of mock galaxies is generated in order to do these tests. As Figure 7 shows, the initial mock galaxy, which has a photometric values of r_e=4, r_{bar}=18 and h=10 arcsec, gets decomposed in bulge, bar and disk.

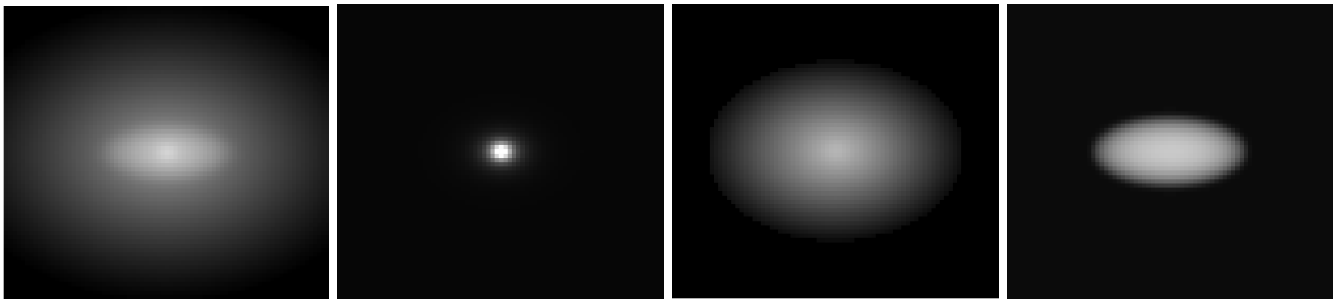

(a) (b) (c) (d)

Figure 7: Mock galaxy created with sizes of the components r_e=4 arcsec, h=10 arcsec and r_{bar}=18arcsec (a). After running C2D over it, the three components are spectro-photometric decomposed in three datacubes, one for the bulge (b), one for the disk (c) and one for the bar (d). All the images are in a logarithmic scale to appreciate the full brightness scale

4.2.1 Profile analysis

Fist of all, due to the uncertainty of having a third component and how this might affect to the other two parts, a set of mock galaxies varying the bar length and keeping fixed the sizes of the bulge and the disk was done. According to the bar dimensions of the CALIFA dataset (Méndez-Abreu et al. 2017) the lowest value for r_{bar} is 4 arcsec and 76 is the largest one, so the first set of mock galaxies consist on several galaxies fixing the sizes of bulges and disks and varying the radius of the bar. The fixed parameters of each component are n_{bar}=n=2, r_e=4 arcsec and h=10 arcsec. The luminosity of each component is also fixed respect to the total luminosity as B/T=0.3, D/T=0.5 and Bar/T=0.2. The inclination of the three components is also fixed to 90º (face-on). In order to generate a given component with the desired age and metallicity, spectra from MILES library are used. This first test (Figure 8 (a)) is made with Z_{bulge}=0.0, Z_{disk}=0.0, Z_{bar}=0.22, Age_{bulge}=1.0 Gyr, Age_{disk}=14.1254 Gyr and Age_{bar}=5.6234 Gyr. Simulations are made with S/N=10 and 1000 ('infinite'), and also simulating them without convolving the images with the typical CALIFA PSF of 2.5 arcsec. This last simulation was made to test how the PSF affects the image of the bulges if these are too small (smaller than the PSF). A second sequence of simulations has been made exchanging the ages of bulge and disk (disk younger than bulge) and using Z_{bulge}=0.4 (Figure 8(b)). From these firsts plots (Figure 8) it can be seen that most of the final age and metallicity values match the initial ones, except for the bulge when r_{bar} has low values ($r_{bar} < 11$ arcsec)(Figure 8 (a)) and for the disk when r_{bar} has high values ($r_{bar} > 20$ arcsec) (Figure 8(b)), both cases affecting the oldest part of the galaxy. The bar below r_{bar}=10 and above 40 arcsec suffers systematical deviations. These deviations in the values are not due to the photometric conditions of the galactic components, so what are they caused for?

To better understand the possible problems related to an inaccurate representation of a real galaxy, it is necessary to check the intensity profiles of the three components and how they could affect each other. Figure 9 represents how the bar intensity profile curve evolves when varying its size, leaving the profiles of the bulge and the disk fixed. From this Figure it is clear that the bar profile can provide unrealistic representation of a galaxy intensity profile with values over the intensity of a bulge. This may cause a problem when it comes to determinate the stellar population of any component whose light profile remains under the bar light curve.

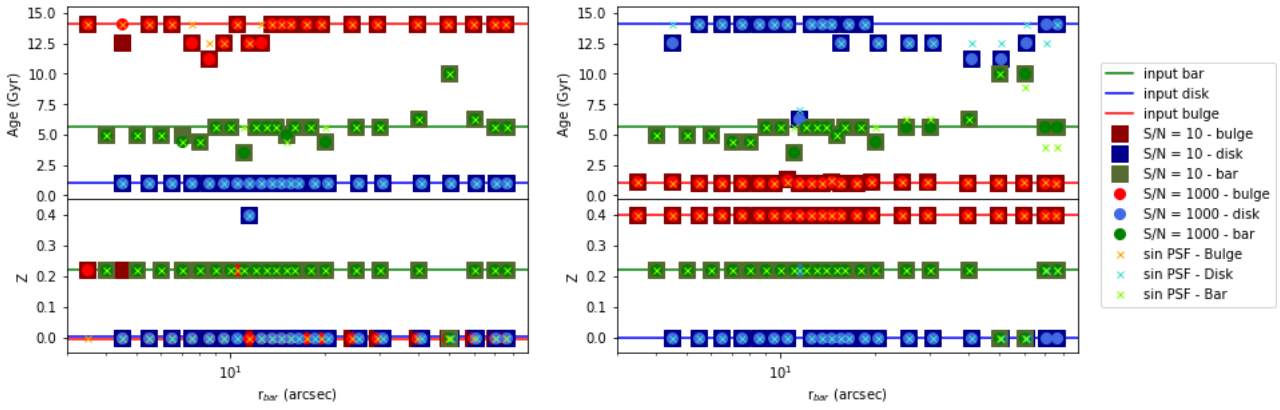

(a) (b)

Figure 8: Values obtained after running C2D on the simulated galaxies and the input values given generating the models with create_cube. In these simulations (a) the bulge is older than the bar and the bar older than the disk and (b) the disk is older than the bar and the bar older than the bulge. Metallicity is supposed to be (a) 0.22 for the bar and 0.0 for the bulge and disk and (b) 0.22 for the bar, 0.4 for the bulge and 0.0 for the disk. The simulations are made with S/N = 10, 1000 ("infinite") and without convolving with the CALIFA PSF(2.5)

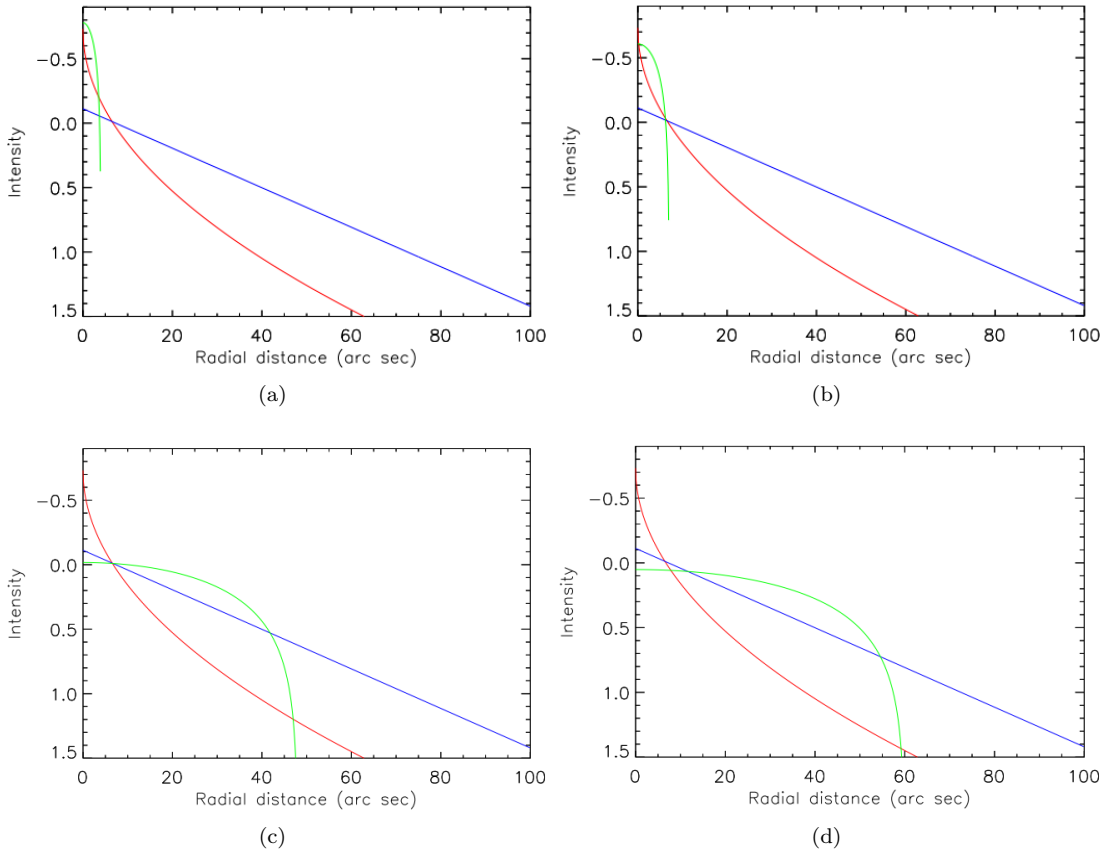

(a) (b) (c) (d)

Figure 9: Intensity profiles for the bulge (red), bar (green) and disk (blue) when the galaxy luminosity configuration is set to B/T=0.3, D/T=0.5 and Bar/T=0.2. The radii of the bulge and disk are fixed to r_e=4 and h=10 arcsec and r_{bar} is 4 (a), 7(b), 48(c) and 60 (d) arc sec.

For a bar with Bar/T=0.2, one of the highest possible, Figure 9 is made. When the bar is short all its luminosity gets concentrated in a small area, what makes it brighter than the bulge. Then, as the bar becomes larger, the bulge stands out more and it could be correctly analyzed. The same thing happens if the bar has a large radius. Its profile is above the disk one so the values for the age and metallicity of the disk can not be well recovered.

This phenomena only happens if the bulge or the disk are the oldest components, because spectra of the young ones is way more different than the older ones. For this reason young components (less than 4 Gyrs) are much more easy to differentiate than the older ones ($\geq$ 5 Gyrs). This is noticeable in Figures 8(a) and 8(b), where the first one (old bulge) has not so accurate bulge values when the bar is short and in the second one in the disk values, when the bar is large. It also happens to be certain values that give some extra error. These values consist on a triple intersection of the profiles in a single point (Figure 9(b) and (c)), which corresponds to the points situated at $\sim$ 12 and 50 arcsec in the r_{bar} values. In these cases the age and metallicity values tend to have a higher deviation from the expected values. Finally, the bar values seem to be inaccurate if its profile is not between the triple intersections of the profiles, as can be seen for the r_{bar} values below 8 and above 40 arcsec.

Knowing this effect, some extra tests were done taking lower values for Bar/T. In these tests, the accurate bar values like the ones observed in Figure 8 happen in a shorter range of r_{bar}, because the first triple point happens later and the second earlier . In the extreme case where the bar profile is below the other two (Bar/T=0.01), there are no good points for the bar but the ones for the bulge and the disk are all correct.

4.2.2 Accuracy on photometric parameters effects

Some tests are performed to know how much an error of 20 % in the photometric parameters measures of the three components affect the right determination of the age and metallicity, so an analysis changing the parameters r_e, h, r_{bar}, n_{bar}, and n_b is done using r_{bar}=18 arcsec, which is the statistically most common value in the CALIFA galaxies and also a value where the three light profiles do not disturb each other (inside the accurate r_{bar} points range). For this set of simulations r_{bar} is fixed and the luminosity of every component is varied from 0.01 to 0.5, leaving the luminosity of the rest of components proportional and coherent to the values above used (while one of the parts is varying between 0.01 and 0.5 the other two have a difference between their luminosities of 0.1 following D/T>B/T>Bar/T). The age and metallicity for the bulge, disk and bar is the same as in the first set of mock galaxies (the bulge is the oldest). The S/N ratio is also varied using the values 10, 20 and 100. In this simulations of mock galaxies, a first set with right measures of the photometric parameters is made (Figure 10) to know if the code is well-behaving if all is set and done properly. The values obtained if the photometric parameters are measured precisely (Figure 10), show that unless the brightness of a determined component is too low (0.01), the values for the age and metallicity of the three components are the same as the ones given creating the mock cubes, except for a pair of deviations in the measures of the bulge (Figure 10(a)) and the bar (Figure 10(b)), which highlights that the error associated with this measures is $\sim$ 1Gyr.

Then the photometric parameters are given $\pm$20 % (maximum error expected of measuring the photometric parameters from the SDSS images) values than the accurate ones to generate the plots of Figure 11, where in each plot only one of the photometric parameters has been modified, leaving the rest with their correct values. These plots are made varying B/T, D/T and Bar/T the same way as in the previous plot. In this case more ages and metallicities of the mock galaxies are not in their supposed value. If the photometric parameter is 20 % lower (Figure 11, right part), this error affects less the age and metallicity datation; the most important case is r_{bar} (Figure 11 (f)), where the metallicities of the bulge and the disk are 0.22 above its expected value. This means that when the bar becomes brighter (and the bulge and disk fainter), the light of the bar affects the correct determination of the metallicities of the other components.

On the other hand, the most important errors noticed are when the free parameters are above its input value (Figure 11, left part) and, one more time, in the r_{bar} part (Figure (e)), where the values of metallicity for the disk are 0.44 above its expected value and the age of the bar is 2.5 Gyr below the age expected. Varying h affects the age of the bar and bulge above D/T=0.1 (the disk does not get affected) and varying the bulge parameters, affects the age of the bulge for all B/T and the metallicity of the disk for high B/T values.

It makes sense that, when the light of the disk is fainter (B/T or Bar/T high), the values of the disk tend to fail and that high values of D/T cause errors in the bar measures. It is also logic that an inexact measure of r_e could lead to fails in the bulge values. The unexpected failing in the bulge age comes when the disk size is above

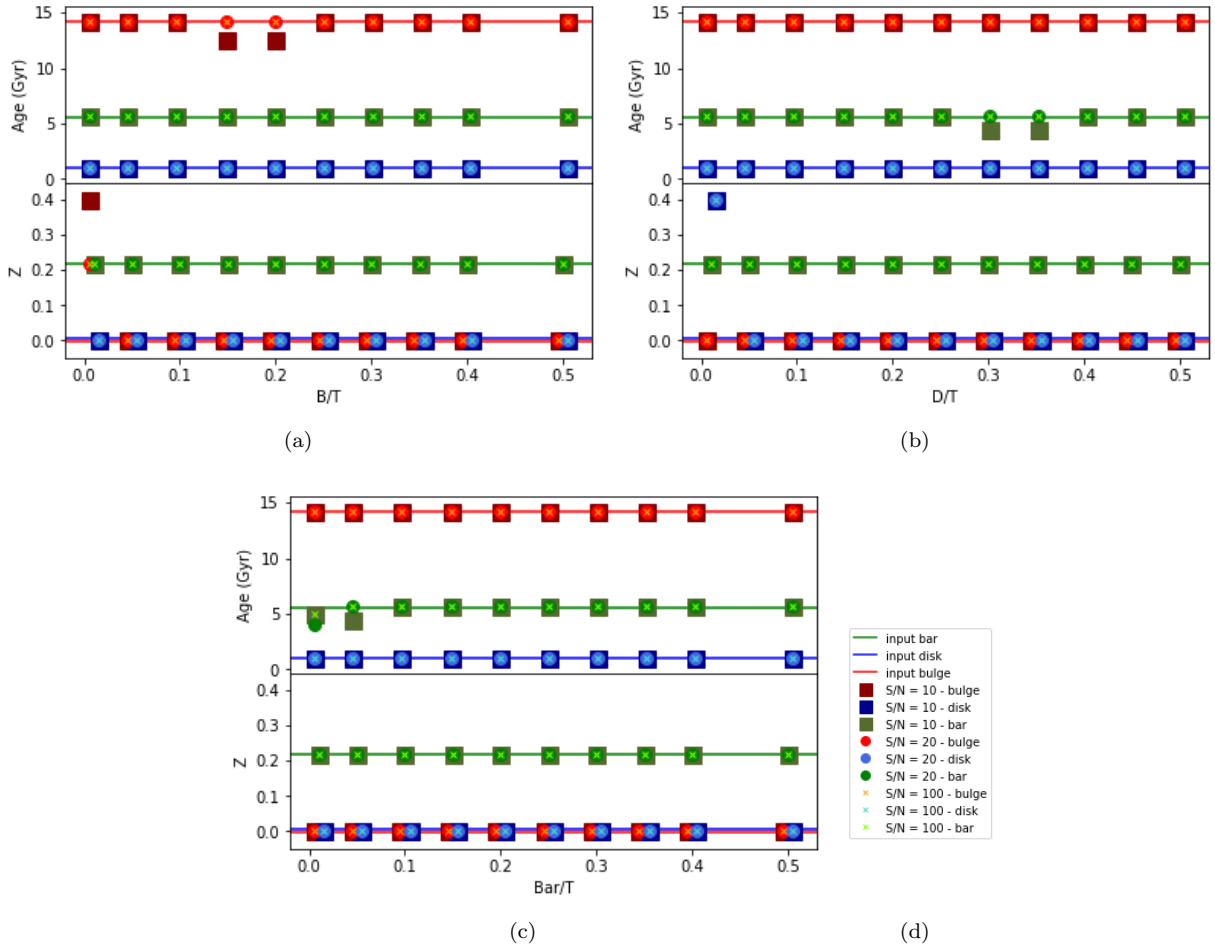

(a) (b) (c) (d)

Figure 10: Values for the age and metallicity of the bulge (red), bar (green) and disk (blue) during the variation of each component luminosity. The mock cubes have been generated with r_e=4.0, h=10.0 and r_{bar}= 18.0 arcsec.

the input value.

After analysing all the possible sources of error and how the C2D code behaves in the different situations, it can be concluded that the component that has more impact in obtaining a precise data is the bar, which can affect the other components when determining their age and metallicity. To see this in detail, a representation of the error with respect to the input value has been made (Figure 12).

As can be seen, the age errors obtained fixing r_{bar} to 18 arcsec are not bigger than 2.5 Gyr and affect mostly the bulge component when the error of 20% is made on the bulge or disk size, and mostly on the bar size when the error is made on the bar size. Otherwise, the age errors obtained when varying the bar radius are more common when the bar has a very large or very small radii and they can reach 5 Gyr in a few cases.

Referring to metallicity, the major problem that can be find is when the luminosity of the disk becomes to small. In this case its error can reach Z=0.4, but otherwise all the measures are quite precise. Varying the bar size, some bad results in the extreme cases can be found, as seen before, when the size of the bar is too short or too large, and mostly on the bar metallicity and a bit less on the bulge metallicity.

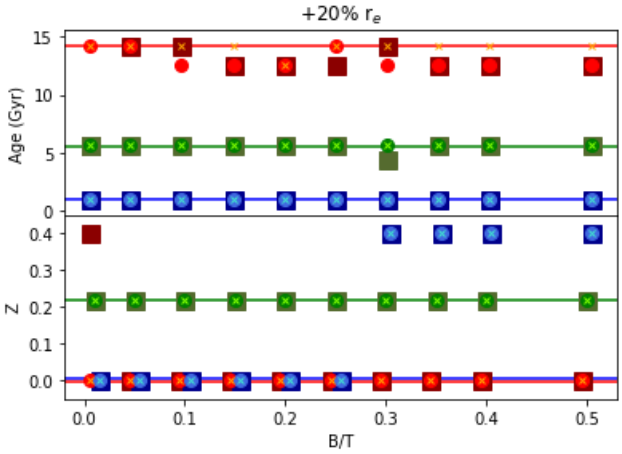
+20% r_e
Age (Gyr)
Z
B/T

(a)

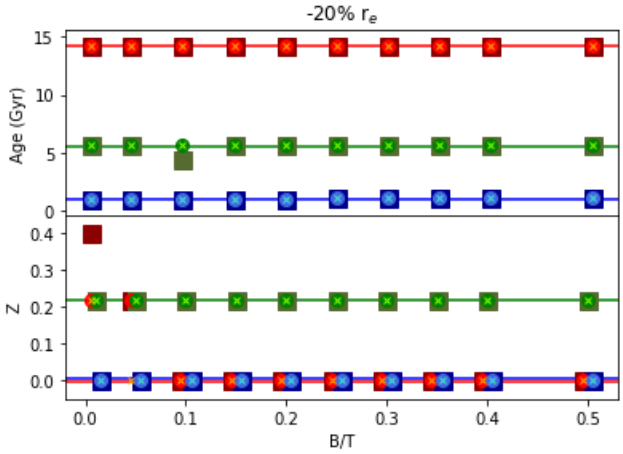
-20% r_e
Age (Gyr)
Z
B/T

(b)

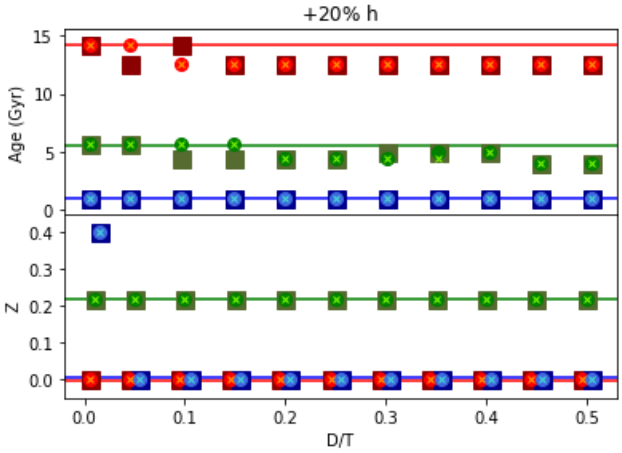
+20% h
Age (Gyr)
Z
D/T

(c)

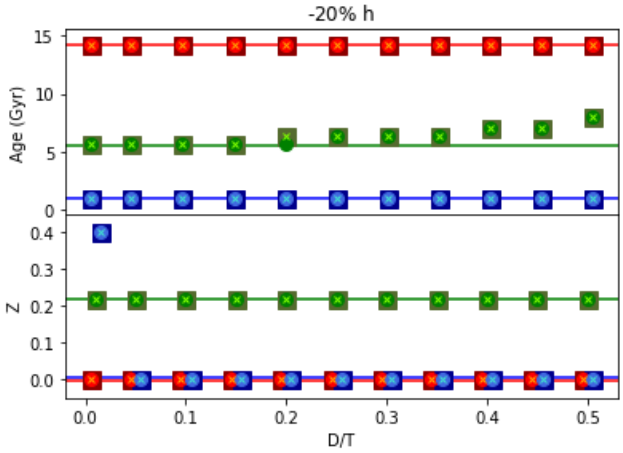
-20% h
Age (Gyr)
Z
D/T

(d)

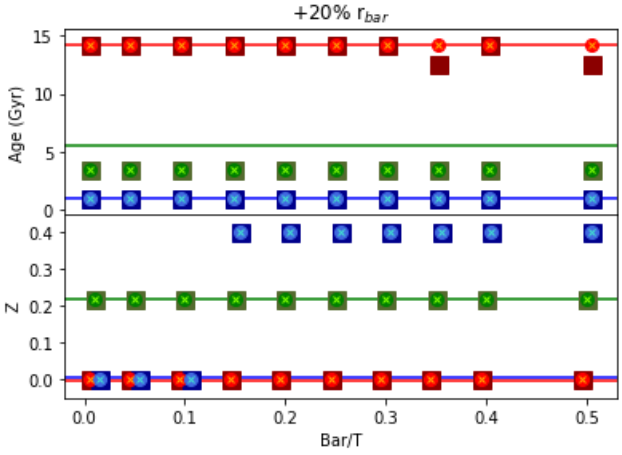
+20% r_{bar}
Age (Gyr)
Z
Bar/T

(e)

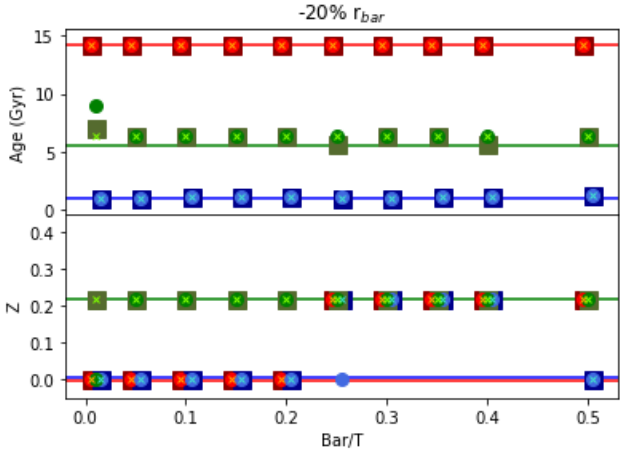
-20% r_{bar}
Age (Gyr)
Z
Bar/T

(f)

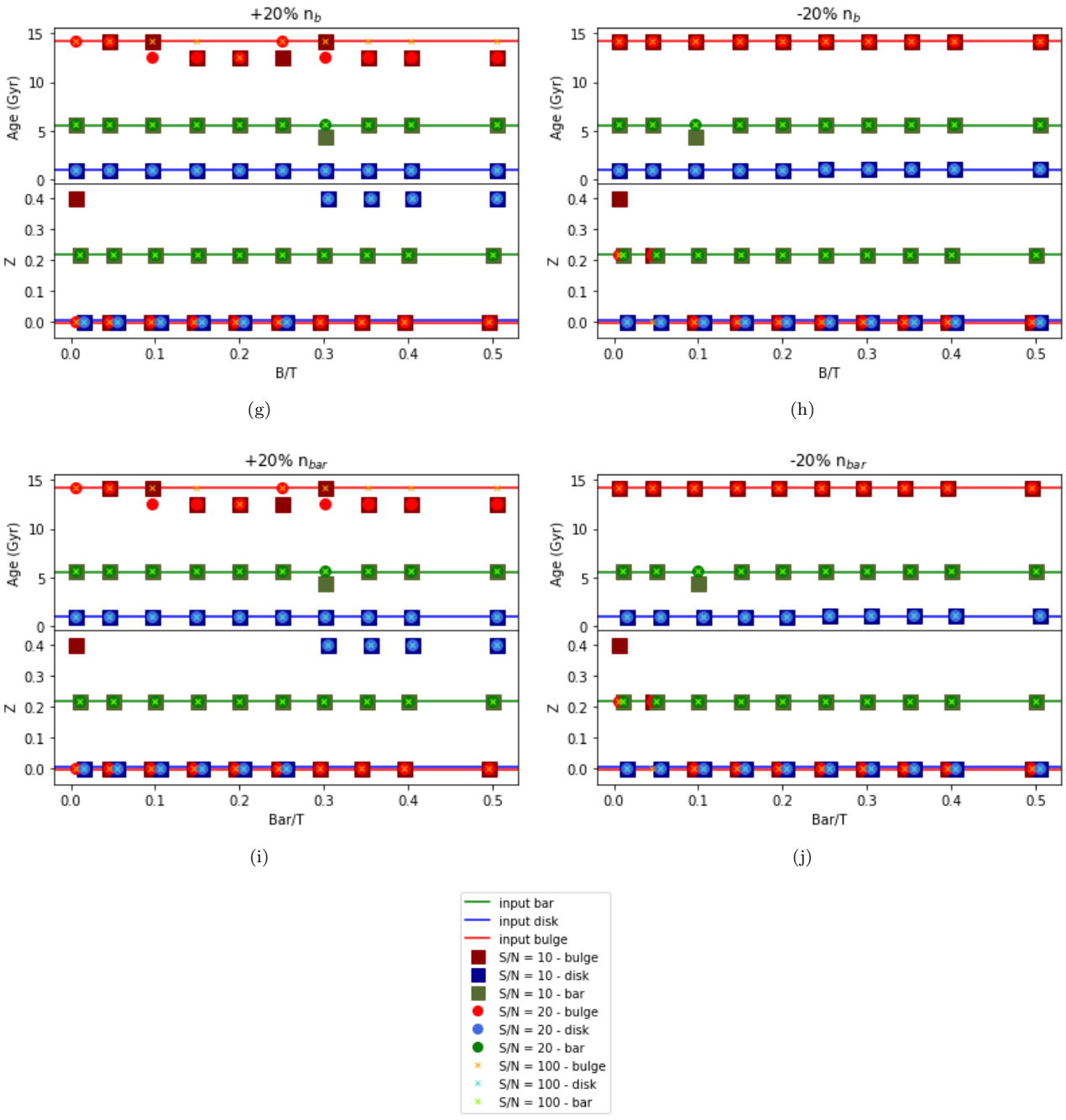

(g) (h)

(i) (j)

(k)

Figure 11: Values for the age and metallicity of the bulge (red), bar (green) and disk (blue) during the variation of each component luminosity. The mock cubes have been generated with r_e=4.0, h=10.0 and r_{bar}= 18.0 arcsec. The parameters fixed in C2D have an intended error in the value of one of the free parameters, above or below the real value, as indicated in the title of each panel.

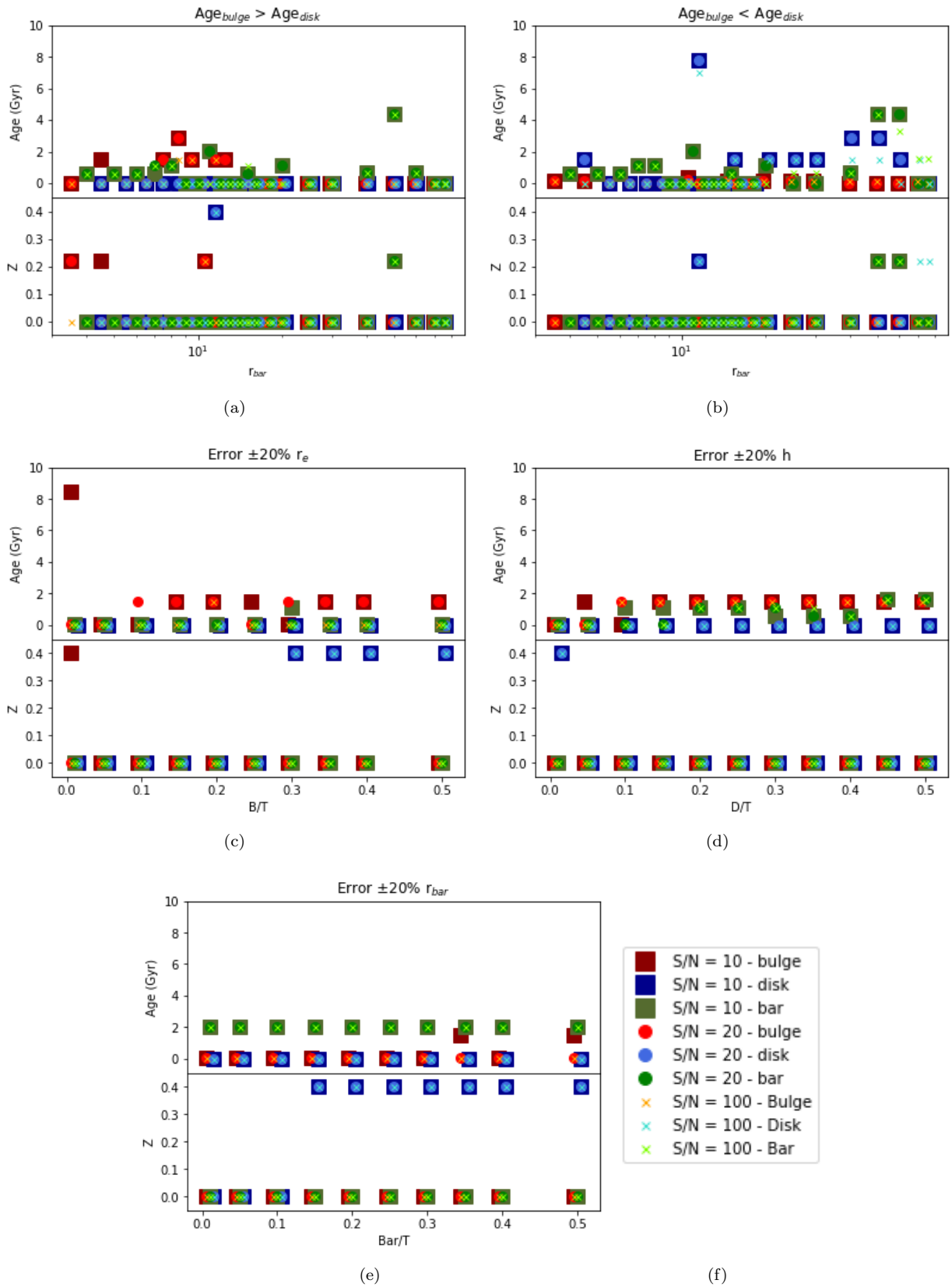

(a) (b)

(c) (d)

(e) (f)

Figure 12: Error in the final measure of the age and metallicity of the three components compared with the input value of the mock galaxies created.

5 CALIFA barred galaxies analysis

A total of 88 barred galaxies from the CALIFA dataset (Figure 5) have been analysed with the C2D code. The results of this analysis are shown in this section. These galaxies have the bulge, disk and bar fitted and do not have truncated disks or a not solved central part.

5.1 Previous steps to spectro-photometric decomposition

Before executing the C2D code over all the galaxies, it is necessary to ensure everything is correctly set to made the decomposition. In the C2D code, the center pixel of each galaxy needs to be set. To take a common center for the galaxy for all the wavelengths, the 2D quasi-monochromatic images are integrated, so the brightest pixel of the final image is taken as the galactic center. This is used along with the 14 photometric parameters obtained from the SDSS images in the three filters (r, g and i) to set all the initial parameters required to run over C2D and GASP2D, in order to do the spectro-photometric decomposition.

After this, it is also necessary to create a mask for the galaxies, given that there are some foreground stars in front of some of the galaxies that need to be masked. In order to do that, the task 'ellipse' from IRAF was used. The images employed to do the masks are obtained by integrating all the wavelengths in each pixel and obtaining a 2D 'white light' image, the same as used before to get the galactic center. Running the task 'ellipse' over this image, all the contaminating objects in it are masked and a mask image is obtained, which will be used when running C2D. Finally, a list of all the galaxies to be decomposed is written, so it can be read by the code to act on all the galaxies in a single run process.

5.2 Decomposition and analysis of the CALIFA barred galaxies

When everything is set, C2D is run over the CALIFA datacubes. All the datacubes are generated and then checked in order to know if they have a good S/N ratio or if they have external stars or galaxies contaminating them. The final datacubes without external objects and good S/N have suffered a satisfactory decomposition, the three components can be distinguished properly in the datacubes for all the wavelengths. A spectrum for each component of each galaxy is also created and it will be used in the next section to be analysed and to obtain the stellar populations of the three galactic parts.

To look for better results when applying pPXF, C2D was run again over some of the galaxies, but instead of fixing the galactic center for all the wavelengths, this parameter was set free in the decomposition process. All the galaxies tested end up the decomposition in good conditions, but the computation time needed for this test was, for each galaxy, two or three times the one needed when the center is fixed. When the new datacubes were used in pPXF, the results and the spectra obtained were not significantly better than in the previous cases. It is true than, in most of the cases, a very small improvement on χ^2 was noticed, but the difference was too small and in some cases one of the other components could get equally, by just a short variation, worse. Just one of the cases, from a list of 20 galaxies tested, presented a really noticeable improvement in its bar spectra S/N, the galaxy NGC0309. Since the computation time needed is much bigger than fixing the galactic center and the results are proven to be quasi similar (the improvement is no significantly relevant), this method has been discarded.

After checking all the galaxies final datacubes and their photometric parameters, such as the brightness of each part, some of the galaxies do not provide a proper spectro-photometric decomposition due to factors such as low S/N or by the fact that B/T or Bar/T have too low values. These factors will affect the analysis of their spectra performed in the next section (see Section 4 for limitations of the method with B/T and Bar/T). The spectra of some components with low values of S/N will not be able to compare them with the templates, so these galaxies were not used to generate the final science plots. The galaxies with low S/N, bad pixels, or with bad photometric parameters are 12: CGCG163-062, ESO540-G003, NGC0976, NGC2558, NGC2565, NGC3815, NGC5056, NGC7691, UGC03253, UGC03995, UGC12348 and UGCA021

5.2.1 Spectro-photometric decomposition of galaxy NGC0364

An example of how C2D does the spectro-photometric decomposition of the bulge, disk and bar parts is shown in Figure 13. To show this, a well-known barred galaxy from the CALIFA dataset is used. NGC0364, whose parameters can be found in Méndez-Abreu et al. (2018). This barred galaxy has a redshift of 0.0166 and a stellar mass of $\log M_\star = 10.674$ $M_\odot$. The bulge parameters are μ_0=19.9, n=1.55 and r_e=0.58 arcsec; the position angles of the disk and bar are PA_d=33.3±0.7º and PA_{bar}91.9±0.4 º

The free parameters of the bulge, disk and bar are fixed using the SDSS multi-band photometric decomposition and then C2D is run over the CALIFA NGC0364 datacube. As it can bee seen in Figure 13, the initial image (a) gets decomposed into its three components (b), (c) and (d). Datacubes of the spectra from every component are also obtained. Characteristic spectra of the three components are also obtained. Analyzing the decomposed images obtained, it can be checked than the decomposition has successfully separated the different components that form the galaxy and each one has coherent values for the surface brightness of the components.

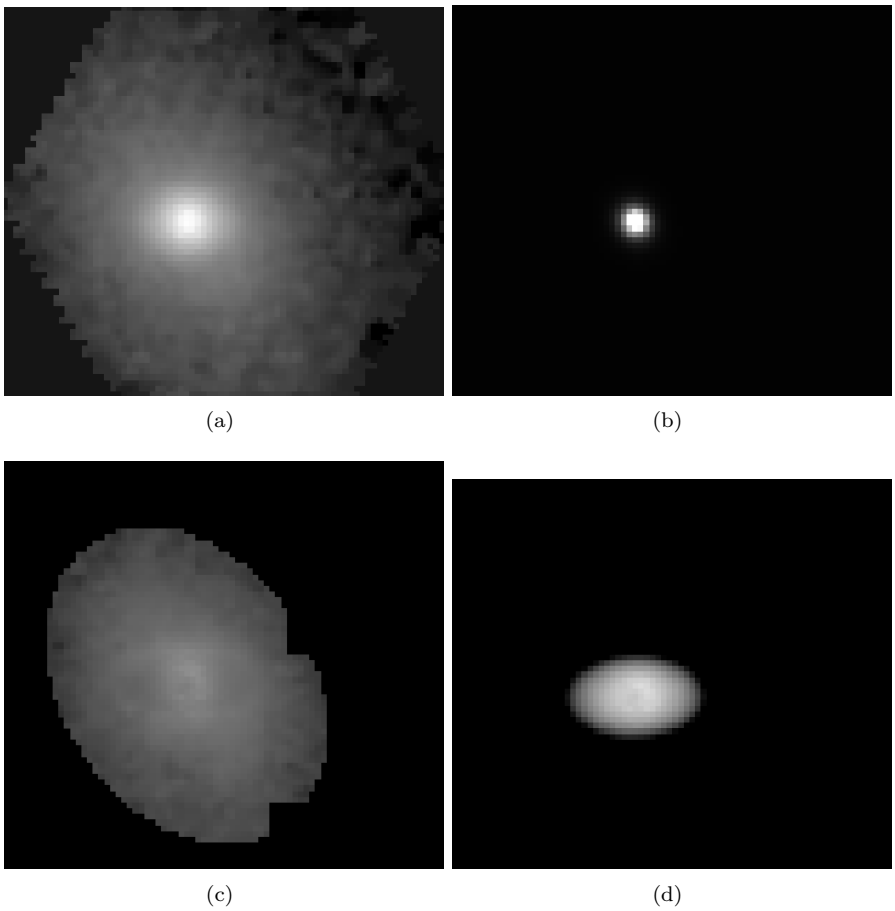

(a) (b) (c) (d)

Figure 13: Datacube from the CALIFA dataset, corresponding to the galaxy NGC0364 (a). After running C2D over it, the three components are spectro-photometric decomposed in three datacubes, one for the bulge (b), one for the disk (c) and one for the bar (d). In the disk image it can be seen the masked parts of the galaxy. All the images are in a logarithmic scale to appreciate the full brightness scale

6 Stellar population analysis of CALIFA barred galaxies

6.1 Using pPXF and MILES templates

The penalized pixel-fitting (pPXF) method is used to extract the stellar and gas kinematics, as well as the stellar population of galaxies, via full spectrum fitting. It was developed by Cappellari & Emsellem (2004) and it is used in combination with the MILES library (Vazdekis et al. 2010). A key feature of pPXF is that it automatically penalizes non-Gaussian solutions, to reduce the noise in the recovered kinematics. pPXF extracts stellar kinematics, performs an emission-line analysis and derives stellar population properties from full spectral, fitting via the measurement of absorption line-strength indices (Cappellari 2017).

The stellar kinematics are extracted by employing as templates linear combinations of a large number (up to a thousand) of template spectra, observed with a different spectrograph than the one used to obtain the galaxy spectra. Due to this difference, before the kinematic extraction, and assuming the templates have a better resolution than the galaxy (CALIFA) spectrum, the templates need to be matched to the galaxy spectrum by convolving them with a kernel which generally varies with wavelength. The templates wavelength range is extracted and logarithmically rebin to the same velocity scale of the CALIFA galaxy spectrum to determine the size needed for the array, which will contain the template spectra. All the templates are oversampled by a factor of two. The mean spatial spectrum obtained for each galactic component is taken and cut to get the waverange between 4400 and 5500 Å. This range begins in the values where the spectra has less noise (bluer values are noisy) until near the 5577 Å sky line, that causes problems fitting the spectra because of its high brightness. Then is also logarithmically rebin to measure velocities from the pixel shift required to match the spectral templates to the galaxy spectrum. This shift corresponds to $\Delta \ln\lambda$, that equals ln(1+z). This is related to Doppler effect by $V \simeq c\ \Delta \ln\lambda$, so a constant velocity scale per pixel can be defined by V=c ln(1+z). This definition is used to convert the pixels differences into velocities, to provide V and σ in km/s.

The pPXF method approximates the observed galaxy spectrum via general parametrization, which adds additive or multiplicative orthogonal polynomials that can significantly minimize template mismatch by changing the strength of individual absorption lines. Additive polynomials can additional correct for imperfect sky subtraction or scattered light. The multiplicative polynomials can correct for inaccuracies in the spectral calibration, and make the fit insensitive to reddening by dust, without the need to adopt a specific reddening curve. To avoid affecting the line strength of the spectral features, additive polynomials are excluded and only multiplicative ones are used, in our case, with a grade 7 polynomial. A set of Gaussian emission line templates is constructed. The lines between 4400 and 5500Å that can be found are Hγ, Hβ and [OIII]5007. pPXF also allows one to fit the gas emission lines together with the stellar kinematics and stellar population. This is achieved by simply passing a set of gas emission-lines templates, together with the stellar ones.

When all these initial parameters are set, the fit starts. The method convolves a linear combination of the template spectra with the galaxies spectra in pixel space by means of a least-squares minimization, seeking to find the set of best-fitting galactic parameters and the corresponding weights. The individual emission-lines are treated as additional Gaussian templates and they are linearly combined with the set of spectral templates to solve for the best-fitting emission-line gaseous kinematics (velocity and velocity dispersion), their strengths (line amplitudes), and weights. The stellar populations are derived on the basis of the linear weights ascribed to the set of template spectra. Small variations in the initial data can translate to large variations in the solution. Thus, regularisation is used to obtain a more physically motivated combination of the spectral template library. The regularisation parameter acts as a proxy for the strength of the regularisation.

During this procedure, but also treating the images in the last section, highlights the fact that all the images have not the same S/N and spatial and spectral resolution. As can be seen in Figure 14, some of the final spectra have a higher noise or the component of the galaxy could not have been well separated and decomposed, so the templates can not be properly fitted.

Even applying the pPXF spectra corrections, some of the galaxies of the dataset were not able to fit one or more components, so the 66 galaxies from the CALIFA dataset used are labeled according to their good fitting with the MILES spectra, for the three components. To have a good fitting means to not have a noisy spectra, so the spectra has a similar shape to the ones from the templates used. The galaxies that are finally taken to do the science plots are the ones with a good fitting in all three components, but all the galaxies in the set are considered in order to do

statistics about how the galaxy characteristics affect to obtain a good galaxy spectrum. The galaxies finally used (with all of their components with good fitting) are 42: IC0679, IC0994, IC4566, NGC0036, NGC0180, NGC0364, NGC0447, NGC0570, NGC0776, NGC0924, NGC1093, NGC1645, NGC2347, NGC2487, NGC2543, NGC2553, NGC2565, NGC2880, NGC3300, NGC3687, NGC5157, NGC5522, NGC5610, NGC5657, NGC5720, NGC5794, NGC5957, NGC6154, NGC6427, NGC6941, NGC6945, NGC6977, NGC7321, NGC7611, UGC01271, UGC03995, UGC04145, UGC08781, UGC09492, UGC11228, UGC11649 and UGC12864.

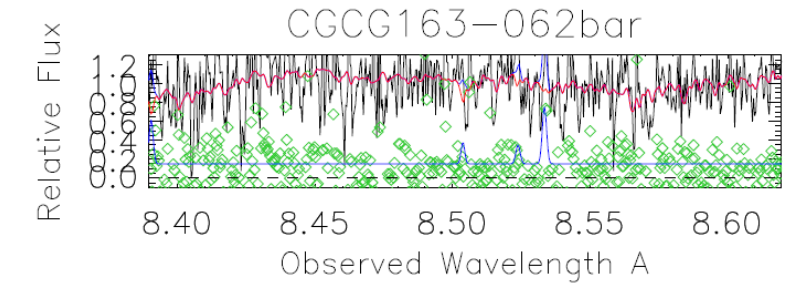

(a)

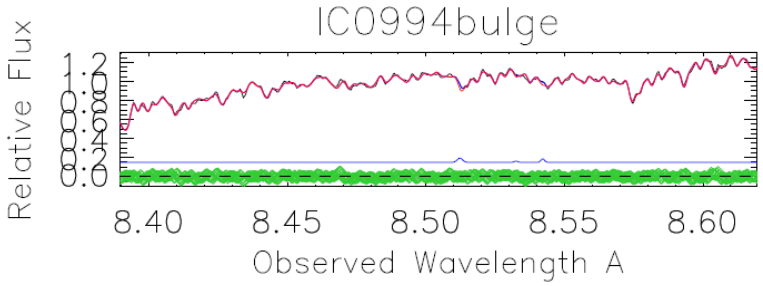

(b)

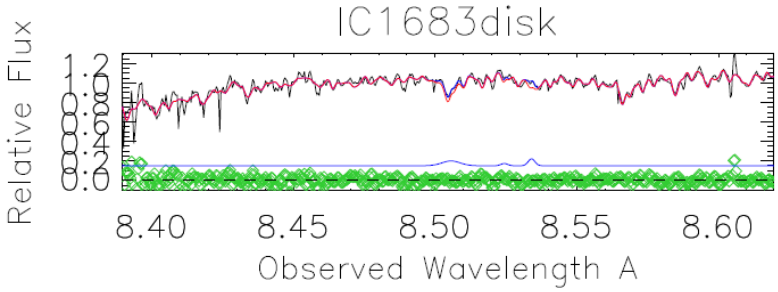

(c)

Figure 14: Examples of the types of spectra fitting found during this work. Average spectra from the datacube in black, best fit spectra from pPXF in pink, emission lines in blue and residuals in green. Type (a) is a noisy spectrum, which usually corresponds to a noisy galaxy that gets completely discarded, type (b) is a good fitting and type (c) is a galaxy with not so much noise as (a) but that has not a good fitting so it is finally discarded.

7 Results

For each galaxy the following parameters are used to obtain the technical and the scientific results: stellar mass of the galaxy, bar ellipticity, and, for each component, 'good fit', luminosity of the component relative to total galaxy luminosity, age, metallicity and size. The stellar mass of the galaxies was obtained from the CALIFA DR3 web page. The bar ellipticity, the luminosity of the component relative to total galaxy luminosity and component size were obtained from the photometry as described in Méndez-Abreu et al. (2017). Finally the good fitting, age and metallicity were obtained using pPXF and the MILES models.

7.1 Setting the limits of C2D with real galaxies

After obtaining all the spectra from the whole set of the CALIFA galaxies used, a visual classification of the spectra fitting was made. The spectra for each component were classified as 'good fit' or 'bad fit' by the criteria seen in Figure 14. After this, a first set of plots are done to test the conditions the galaxy should have to get the best spectrum possible. In this analysis all the galaxies are used, but the ones with better S/N ratio in any component are used to remark which is the best possible scenario that can be found.

First, the luminosity ratio from each component is studied. Obviously, the more light received, the less noisier the spectrum of a component is. This can be appreciated in the Figure 15, where the best spectra obtained are the ones with the higher relative luminosity. The problem is that if one component, usually the disk, has most of the light of the galaxy, this makes the other two fainter and with a lower S/N ratio, so the ideal case is to have a balance between the three parts. The best bulge case is to have a minimum value of 0.05 above the total luminosity and the bar to have at minimum of 0.1, this leaves the disk with a value a little lower than 0.9, which is a favorable case most of the times. These brightness conditions will be the ones expected for the galaxies in order to have the best spectrum possible, otherwise one or more of the components would be too noisy and a complete and trustful determination of the age and metallicity will not be possible.

The limiting values obtained here for the real galaxies are in good agreement with those derived using mock galaxies in Section 4. The expected value of B/T to get a good fit from simulations was above 0.01 (see Figure 10) and here is above the same value (Figure 15(a)), where the number of good fitted galaxies is higher than the bad fitted ones.

7.2 The age and metallicity of bulges, bars and discs in CALIFA barred galaxies

This second set of results are made by just taking the best galaxy spectra, the ones with the lower noise. With the information obtained from this part, the formation and evolution of the barred galaxies are expected to be clarified. The first things to look at are the ages and metallicities of the three components.

From Figure 16 it can be seen that the values of the three component ages are quite distributed along all the age range (mostly between 4 and 15 Gyrs). In this wide range, the disks tend to be slightly older than the bulge and bar. Table 1 shows that the mean ages of the three components are very similar and quite old, given that the range of ages is quite wide. On the metallicities, disks tend to be more metal-poor, with bulges covering the higher metallicity values and bars having an intermediate value. As seen in Figure 16 (b), the more metal-rich component is usually the bulge, followed by the bar. This could imply that disk stars formed from a less metal-rich gas.

From the Figure 17 (b) it can be appreciated than the metallicity difference between disks and bulges/bars (maximum around 0.2) is higher than between bulges and bars (maximum around 0), leaving between them a peak corresponding to the difference between bars and disks (around 0.1). The disks are expected to be the less metal-rich and the bulges to be the most (van Dokkum et al 2010), so it makes sense that the major differences are shown between bulges and disks. On the other hand, it is found that bars tend to be more similar to bulges in terms of their ages and metallicities (as seen in the small bar-bulge age deviations in Figure 17 (a) and (b)). It is known that the gas inflow mechanism allows the bar to take gas and stars from the disk and possibly induce some recent star formation in the galaxy center. This can be related with the bulge-bar metallicity difference being the one with the smallest values in Figure 17(b), but also having an important number of galaxies with higher bulge-bar metallicity differences. The age differences follow a similar trend. The disk-bar/bulge are the major age differences and the minor ones are the bar-bulge differences. The age differences of the galaxy components, in average, are not bigger than a few Gyrs, which indicates that bars act as intermediary between disks and bulges, triggering star formation in bulges making them to be younger or having a similar age than the disks.

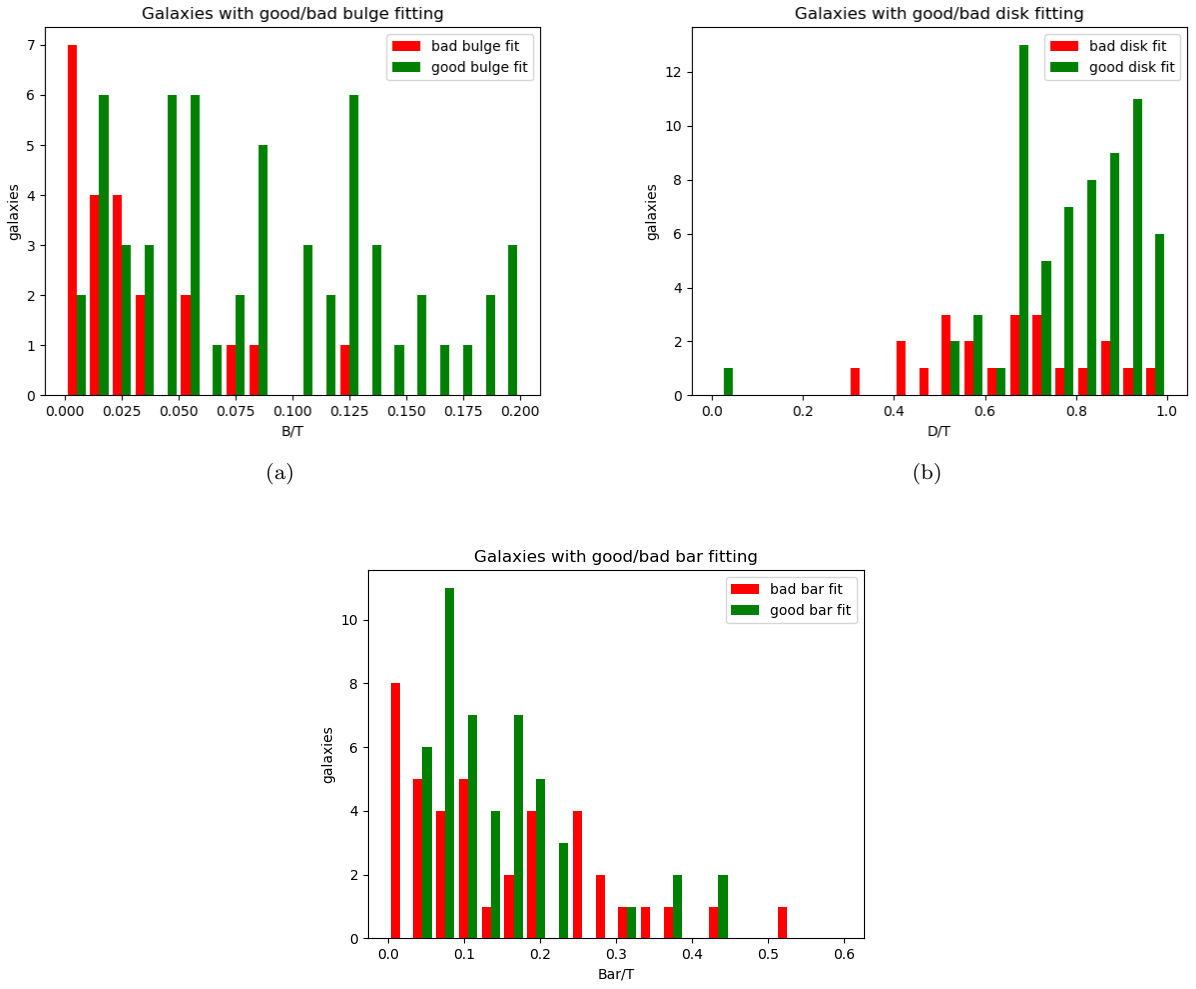

(a) (b) (c)

Figure 15: Distribution of the bulge (a), disk (b) and bar (c) luminosities relative to the total galaxy luminosity. In each plot the galaxies are divided in two groups, one where the components have high S/N ratio, called good fit (green) and the ones which are too noisy, called bad fit (red).

7.3 The relation between stellar populations and morphology

With all the photometric data acquired, some extra information could be obtained. In Figure 18 (a) it is represented the luminosity ratio of the galaxy bulges and how this relates with their ages. Here there is no clear dependence between the two parameters, although it could be guessed that the bulges with high luminosity ratios tend to be older while the ones with low B/T have a wide range of ages. Figure 18 (b) represents how B/T is related to the bar ages. Again, it seems not to be a clear relation, but it could be guessed that the more luminous the bulge, the older the bar. The Figure 18 (c) represents the relation between the bar age and the component ellipticity. This does neither show any particular slope, even if numerical models show that the ellipticity of the bar is supposed to grow as the bar becomes older. This can be intuited in the central part of the plot, where the density of points is slightly bigger, but the huge dispersion of the rest of the points makes impossible to reach to a clear conclusion.

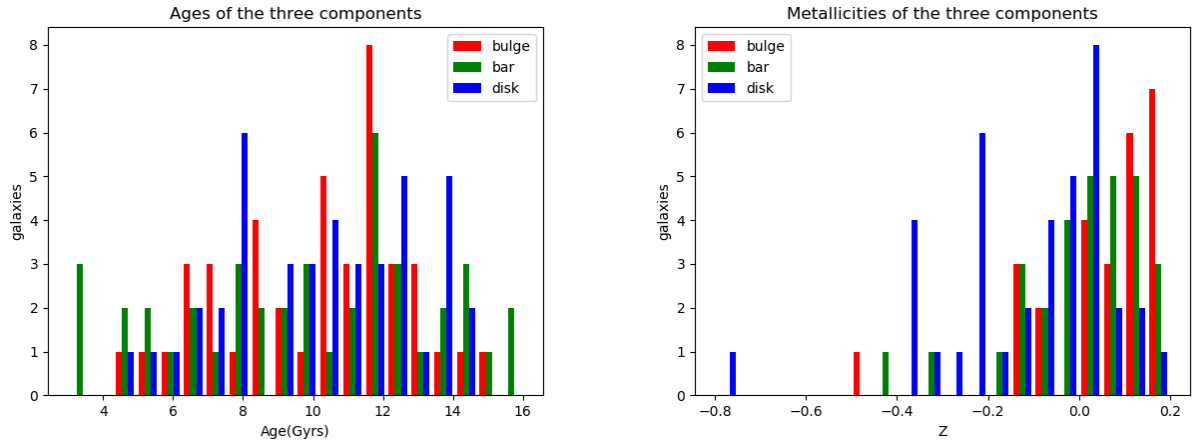

(a) (b)

Figure 16: Distribution of the age (left panel) and metallicity (right panel) for the different components (bulge, bar and disk) of our sample of good fit galaxies. In each plot the values of the bulge are represented by the red values, the disk values are the blue ones and the bar ages and metallicities are painted in green. This set of galaxies are the ones with higher S/N ratio in all the components.

	bulge	disk	bar
mean age value (Gyr)	10.108	10.219	9.889
age standard deviation (Gyr)	2.5458	2.678	3.554
mean metallicity value	0.112	-0.106	0.063
metallicity standard deviation	0.141	0.226	0.153

Table 1: Mean values of the ages and metallicities of the galactic components and their standard deviation value.

An analysis on how age and metallicity vary depending on the photometric parameters of each galactic component is also done. In Figure 19 (a) and (b) is shown how the age and metallicity of the three components vary depending on the bulge luminosity ratio. The trends observed suggest that the galactic components seem to become older as the luminosity ratio of the bulge increases, while the bulges and bars become more metal-rich and the disks more metal-poor. Under these panels, representing the age and metallicity dependence on the bar luminosity ratio (Figure 19 (c) and (d)), it can be seen that the luminosity ratio of the bar does not seem to have a clear relation with ages and metallicities, all the points have a wide dispersion and there is no noticeable trends such as in the previous panels.

Looking at the sizes of the three components and their relation to the stellar populations of the galaxy components, Figure 20 (a) and (b), which show how ages and metallicities depend on the bulge size, as well as Figure 20 (c) and (d), which shows the same but depending on the disk size, seem to indicate that these photometric components do not have an impact on the stellar populations of any galactic component. In a closer look, the bulges could be more metal-rich than the disks for bigger size bulges. In the case of the age and metallicity depending on bar size (Figures 20 (e) and (f)), the metallicities remain not disturbed by the bar length (bulges and bars are usually more metal-rich than disks), while the age trend suggest that as the bar grows the bulges tend to be younger and the disks, older. This could be caused by the bar effects, that could have quenched star formation in the disk (so they become older) and produce a later burst in the inner parts of the galaxy, which could lead to the formation of young stars in the bulge.

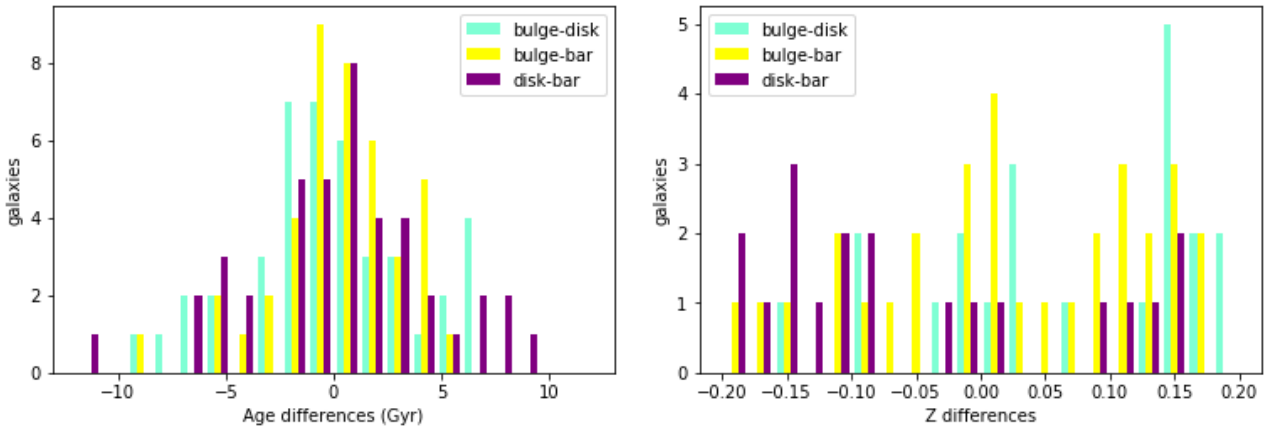

(a) (b)

Figure 17: Distribution of the age (left panel) and metallicity (right panel) differences between components (bulge, bar and disk) of our sample of good fit galaxies. In each plot the values of the bulge-disk difference are represented in light blue colour, the bulge-bar values are the yellow ones and the disk-bar ages and metallicities are shown in purple. This set of galaxies are the ones with higher S/N ratio in all the components.

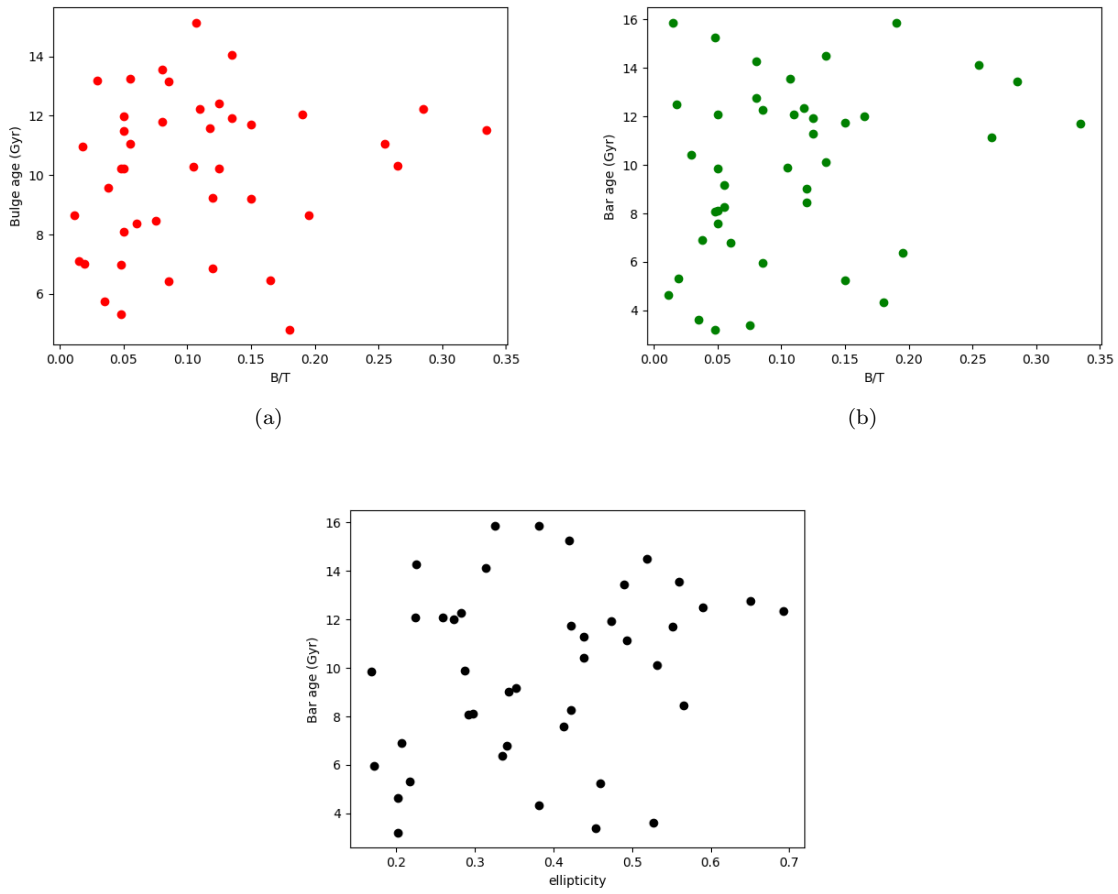

(a) (b)

(c)

Figure 18: Bulge (a) and bar (b) ages depending on the luminosity of the bulge respect to the galaxy total luminosity, and bar age depending on the ellipticity of the bar (c).

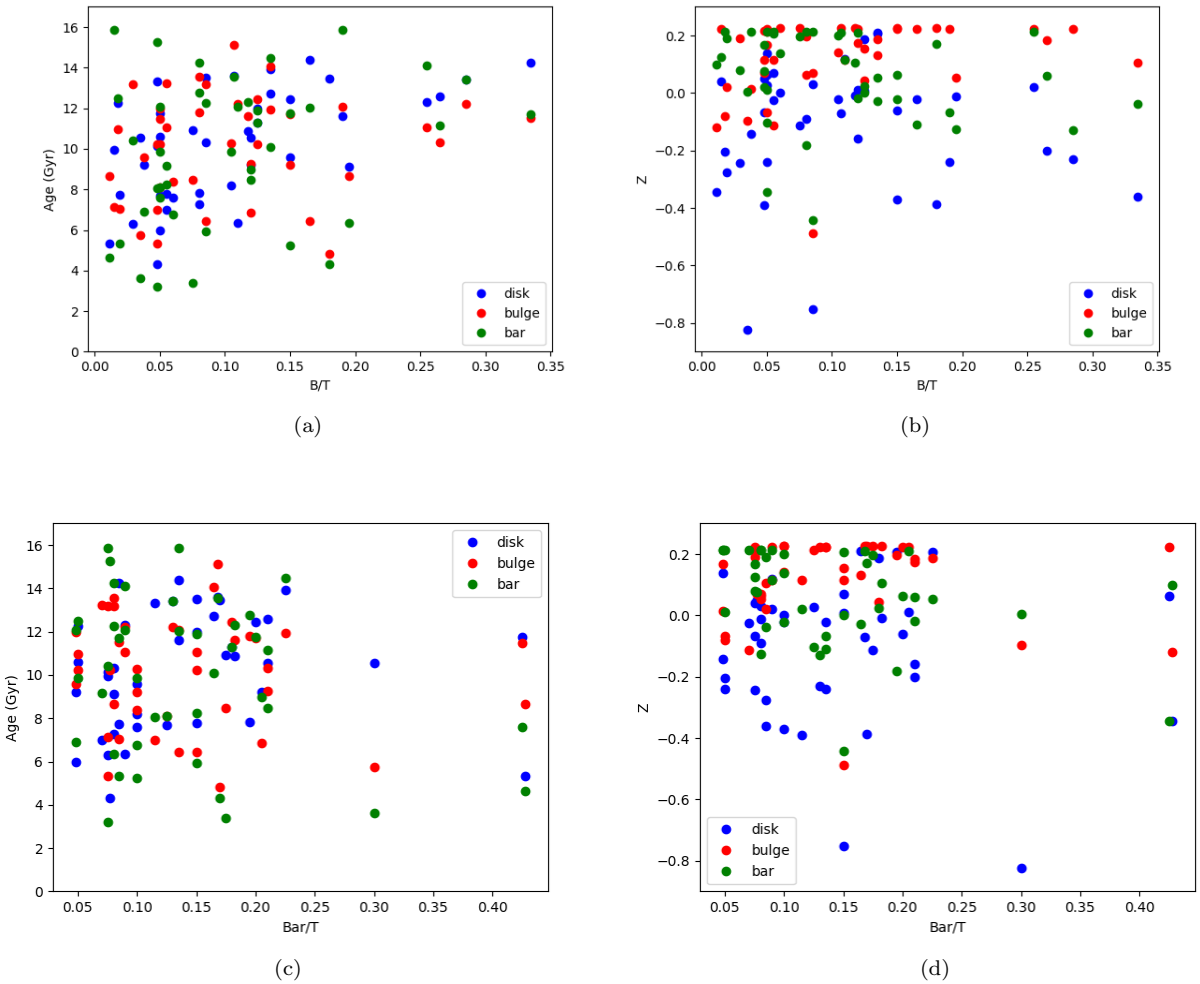

Figure 19: Ages and metallicities of bulge (red), disk (blue) and bar (green) for each galaxy depending on the bulge, (a) and (b), or the bar, (c) and (d), to total luminosity ratio.

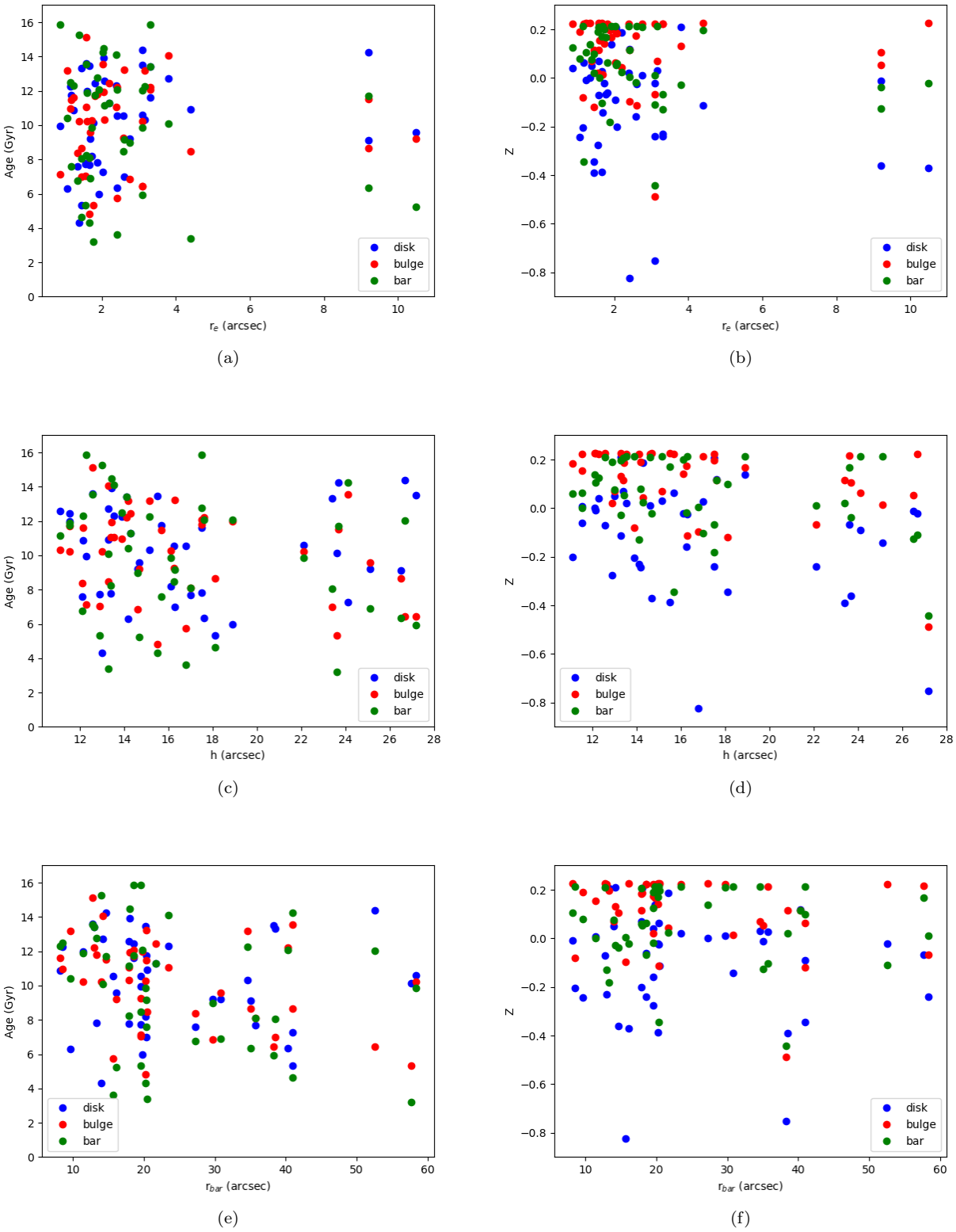

Figure 20: Ages and metallicities of bulge (red), disk (blue) and bar (green) for each galaxy depending on the bulge size, (a) and (b), on the disk size, (c) and (d), and bar size, (e) and (f).

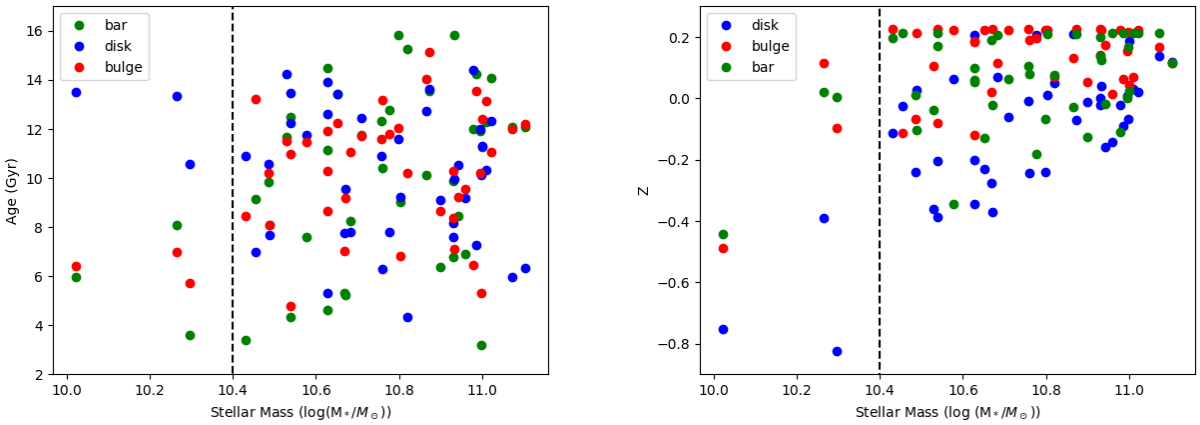

(a) (b)

Figure 21: Ages and metallicities of bulge (red), disk (blue) and bar (green) for each galaxy depending on the stellar mass of the galaxy.

7.4 The influence of the galaxy stellar mass on the stellar structures of barred galaxies

The next thing to consider is how the total stellar mass of the galaxy influences the stellar populations properties of the different components in our galaxies. In Figure 21 a clear separation in all the points is appreciable. When the logarithm of the stellar mass is below $\log(M_*/M_\odot) \sim 10.4$ there is an important change in the behavior of the data. Despite the lower number of galaxies for less massive galaxies ($\log(M_*/M_\odot) < 10.4$), some tendencies appear. Disks are always more metal-poor than bars and bulges for any stellar mass value, but the disks seem to follow the typical mass-metallicity relation observed for star-forming galaxies, and already described for CALIFA galaxies in Gonzalez-Delgado et al. (2014). On the other hand, bars and bulges do not have this trend when the logarithm of the stellar mass is above $\log(M_*/M_\odot) \sim 10.4$, the increase stops and their metallicity values remain constant. The $\log(M_*/M_\odot) \sim 10.4$ values also set a change on the behavior of the ages of the three components. The ages of the components above $\log(M_*/M_\odot) \sim 10.4$ are mixed, so there are no components clearly younger than other ones, but below $\log(M_*/M_\odot) \sim 10.4$, the disk appears to become older than the other two components

8 Discussion and conclusion

The first part of this work is based on improving the C2D algorithm by adding the bar component and testing how this new structure affects all the spectro-photometric decomposition process, and the two other components. For this purpose, the C2D code has been modified to include a bar component fitting

After this, mock galaxy simulations have been made. This mock galaxies are created with observational and physical parameters to emulate the ones from the CALIFA set, and their stellar populations have been characterized using the MILES library. Part of this work has been to modify the code that generates the mock galaxies to add the bar part. Several sets of mock galaxies, with different photometric parameters for each of the three galactic components, have been generated to test how the accuracy in the measure of these parameters results in higher errors when recovering the stellar populations. Another code to recover the stellar populations taking as input the spatially averaged spectra of the spectro-photometric decomposed components has been also modified to include the bar part during this thesis work. It has been found that the bar component light profile can disturb the bulge and disk ones, mostly when the bulge or the disk have a similar or older age than the bar (the bulge for short bar sizes and the disk for larger ones), and the light profile of the bar has higher values than the light profiles of the bulge and the disk. Not considering the bar size problems (having one that do not alter bulge and disk stellar populations), it has also been tested the possible issue of not having accurate input measurements for all the photometric parameters (obtained from SDSS images). The tests with the mock galaxies have been performed increasing or decreasing the luminosity ratios of bulge, disk and bar, leaving the rest of photometric parameters in their correct values and then increasing or decreasing 20 % the input photometric parameters used to generate the mock galaxies, while also varying the luminosity ratio of the three galactic components. The results demonstrate that low luminosity components (luminosity ratio below 0.01) could return bad age and metallicity values. Along this line, it is also found that the photometric parameters that could produce the higher age and metallicity measuring errors are the bar ones, and that obtaining photometric parameter deviations above the correct values generates higher errors than the deviations under them. The simulations varying the photometric parameters show that the errors obtained when retrieving the age and metallicity values could reach near 2.5 Gyrs in the worst cases, but if the photometric parameters measure is quite precise, this error reduces to 1 Gyr.

A set of 88 CALIFA barred galaxies has been selected considering them not to have truncated disks or a not solved central component. After the mock galaxies tests, the C2D algorithm has been tested in a well-known CALIFA galaxy, NGC0364, to ensure the spectro-photometric decomposition separates bulge, bar and disk, obtaining good results. After this last test, C2D was run over all of the CALIFA galaxy set, obtaining the spatially resolved datacubes for bulge, disk and bar. Some of them happened to have low S/N ratio imaging or bad photometric parameters, so 12 of them were excluded. Then pPXF was run over each galactic component spatially averaged spectrum to obtain their stellar populations. Some of these spectra were also discarded because of their low S/N ratio, leaving a total of 42 galaxies to be used to obtain the science results.

The usual scenario for a spiral galaxy to be formed, as seen in Section 1, would be to grown inside-out. The bulge is formed first at a high redshift and then, by accreting gas from a merging process or from the interstellar medium, the disk is formed. This is in agreement with most results obtained from the CALIFA survey for galaxies at low redshift (Gonzalez-Delgado et al. 2017, 2016), where the outer parts of the galaxies are younger and more metal-poor than the central ones. If the disk is cold enough, a bar could be formed, which would have an age and metallicity similar to the disk. As the time goes by, the galaxy is accreting gas and forming new stars, but just in the disk part, what makes it look younger and more metal-poor then the other two components already formed. During this time the bar might be redirecting part of the disk gas into the bulge (by loosing of angular momentum). This drives to new star formation in the bulge, modifying its shape or even creating it, so this makes the bulge look younger and less metal-rich.

What is shown in the results (Figure 21) indicates that the more massive galaxies ($\log(M_*/M_\odot) > 10.4$) do not accrete much more metal-poor gas after they are formed, so the three components remain with age and metallicity values quite similar along this mass range, being the disks usually more metal-poor than the bulges and bars. This can be, somehow, also seen in SDSS color images shown in Figure 5, where it can be seen that most of the galaxies are quite reddish for all three components. In Figure 18 (a) and (b), it can be intuited a trend where the more luminous bars and bulges (B/T and Bar/T > 0.2), are the ones with older ages, corresponding to the more massive galaxies, while the lower B/T and Bar/T values have a huge variety of ages for both bulge and bar. In

contraposition, the results suggest that less massive galaxies ($\log(M_*/M_\odot) < 10.4$) accrete gas at later stages of the galaxy history, causing the disks to be much more metal-poor. This gas could have also been redistributed in the inner parts of the galaxy, that is why, despite the disks being more metal-poor, the bar and the bulge end up being younger (Figure 21). This might be also backed up by looking at Figure 20 (e) and (f), where the larger bars, that can take more gas from the disk due to their larger torques, trigger the nuclear star formation leading to younger bulges and quenching star formation in the inner parts of the disk, creating a region called "Star Formation Desert" (SFD; James et al. 2009; James & Percival 2016; Donohoe-Keyes et al. 2019). In this region, the star formation in the disk part within the bar radius but outside the bar is suppressed rapidly after the bar formation.

The results obtained in this work present new information on the possible formation of barred galaxies. They point to a complex mixture of processes acting on each galaxy. Despite the fact that usually the disks are more metal-poor than the central parts of the galaxies, they have been found to be the oldest component in most galaxies, which, apparently, is in conflict with the inside-out galaxy formation scenario. However, the age ranges of the components are broad, so the effects of the bar on creating or modifying the bulge or even its own star formation can produce the mixture of stellar populations obtained in this study.

9 Future work

There are some aspects of this work that can be improved in order to look for more accurate results or more specific studies about the galactic stellar populations.

To better obtain the values of the stellar populations for each component, a more detailed analysis of the regularization in the pPXF code could be done. In this work, the procedure followed was to fix the value of the regularization to a standard value and to use it when fitting all the galaxies. It might be considered that each galaxy and each galactic component could need a different value for this parameter, so a future study with the regularization adjusted to each component could lead to more precise results and with them having a possible higher S/N rate.

Due to the restrictions in time and to the great amount of data that has been used and analyzed, a detailed analysis of the pPXF fitting method associated errors could not be performed. The errors of the component stellar populations have been obtained from the mock galaxy simulations, estimating the errors associated to the measures of the galaxy photometric parameters. A study of the age and metallicity errors that can be derived from the pPXF fitting method would give a more precise picture of the final stellar population measures for each galactic component.

In this work the component spectra used were the averaged spatial ones, but it has to be considered that each component has age and metallicity spatial variations, especially in the disks, where the bar could affect their inner stellar populations. To do a study analysing also this component spatial variations could lead to a better understanding of the formation and evolution of the barred galaxies, and how the bars condition the stellar populations of disks and bulges.

References

[1] Abraham, R. G. et al. 1996 "Galaxy morphology to I=25 mag in the Hubble Deep Field" Monthly Notices of the Royal Astronomical Society, Volume 279, Issue 3, pp. L47-L52.

[2] Aguerri, J. A. L. et al. 2009 "The population of barred galaxies in the local universe. I. Detection and characterisation of bars" Astronomy and Astrophysics, Volume 495, Issue 2, 2009, pp.491-504

[3] Aguerri, J. A. L. et al. 2005 "Photometric properties and origin of bulges in SB0 galaxies" Astronomy and Astrophysics, Volume 434, Issue 1, April IV 2005, pp.109-122

[4] Athanassoula, E. et al. 2013 "Bar formation and evolution in disc galaxies with gas and a triaxial halo: morphology, bar strength and halo properties" Monthly Notices of the Royal Astronomical Society, Volume 429, Issue 3, p.1949-1969

[5] Athanassoula, E. 2002 "Formation and Evolution of Bars in Disc Galaxies" Disks of Galaxies: Kinematics, Dynamics and Peturbations, ASP Conference Proceedings, Vol. 275. Edited by E. Athanassoula, A. Bosma, and R. Mujica. ISBN: 1-58381-117-6. San Francisco: Astronomical Society of the Pacific, 2002, pp. 141-152

[6] Balcells, M. et al. 2007 "Galactic Bulges from Hubble Space Telescope NICMOS Observations: Central Galaxian Objects, and Nuclear Profile Slopes" The Astrophysical Journal, Volume 665, Issue 2, pp. 1084-1103.

[7] Brazza, F.D. et al. 2008 "Bars in Disk-dominated and Bulge-dominated Galaxies at z $\simeq$ 0: New Insights from 3600 SDSS Galaxies" The Astrophysical Journal, Volume 665, Issue 2, pp. 1084-1103.

[8] Barrera-Ballesteros, J. K. et al. 2014 "Kinematic alignment of non-interacting CALIFA galaxies. Quantifying the impact of bars on stellar and ionised gas velocity field orientations" Astronomy & Astrophysics, Volume 568, id.A70, 30 pp.

[9] Benítez, E. et al. 2013 "Characterization of a Sample of Intermediate-type Active Galactic Nuclei. II. Host Bulge Properties and Black Hole Mass Estimates" The Astrophysical Journal, Volume 763, Issue 2, article id. 136, 13 pp.

[10] Berentzen, I. et al. 2003 "Numerical simulations of interacting gas-rich barred galaxies: vertical impact of small companions" Monthly Notice of the Royal Astronomical Society, Volume 341, Issue 1, pp. 343-360.

[11] Boselli, A. and Gavazzi, G. 2014 "On the origin of the faint-end of the red sequence in high-density environments" The Astronomy and Astrophysics Review, Volume 22, article id.74, 58 pp.

[12] Bournaud, F. et al. 2007 "Rapid Formation of Exponential Disks and Bulges at High Redshift from the Dynamical Evolution of Clump-Cluster and Chain Galaxies" The Astrophysical Journal, Volume 670, Issue 1, pp. 237-248

[13] Bournaud, F. et al. 2005 "The lifetime of galactic bars: central mass concentrations and gravity torques" Monthly Notices of the Royal Astronomical Society: Letters, Volume 364, Issue 1, pp. L18-L22.

[14] Buitrago, F. et al. 2008 "Size Evolution of the Most Massive Galaxies at 1.7 $<$ z $<$ 3 from GOODS NICMOS Survey Imaging" The Astrophysical Journal Letters, Volume 687, Issue 2, pp. L61

[15] Cappellari, M. 2017 "Improving the full spectrum fitting method: accurate convolution with Gauss-Hermite functions" Monthly Notices of the Royal Astronomical Society, Volume 466, Issue 1, p.798-811

[16] Cappellari, M. and Emsellem, E. 2004 "Parametric Recovery of Line-of-Sight Velocity Distributions from Absorption-Line Spectra of Galaxies via Penalized Likelihood" The Publications of the Astronomical Society of the Pacific, Volume 116, Issue 816, pp. 138-147.

[17] Carollo, C. M. et al. 2007 "Old and Young Bulges in Late-Type Disk Galaxies" The Astrophysical Journal, Volume 658, Issue 2, pp. 960-979

[18] Carrasco, E.R. et al. 2010 "Gemini K-band NIRI Adaptive Optics Observations of massive galaxies at 1 $<$ z $<$ 2" Monthly Notices of the Royal Astronomical Society, Volume 405, Issue 4, pp. 2253-2259

[19] Ciambur, B.C. et al. 2020 "Double X/Peanut Structures in Barred Galaxies – Insights from an N –body Simulation" eprint arXiv:2003.00015

[20] Cid Fernandes, R. et al. 2014 "Resolving galaxies in time and space. II. Uncertainties in the spectral synthesis of datacubes" Astronomy & Astrophysics, Volume 561, id.A130, 19 pp.

[21] Cid Fernandes, R. et al. 2013 "Resolving galaxies in time and space. I. Applying STARLIGHT to CALIFA datacubes" Astronomy & Astrophysics, Volume 557, id.A86, 15 pp

[22] Cisternas, M. et al. 2015 "The Role of Bars in AGN Fueling in Disk Galaxies Over the Last Seven Billion Years" The Astrophysical Journal, Volume 802, Issue 2, article id. 137, 10 pp.

[23] Colpi, M. 2014 "Massive Binary Black Holes in Galactic Nuclei and Their Path to Coalescence" Space Science Reviews, Volume 183, Issue 1-4, pp. 189-221

[24] Combes, F. 2011 "Pattern speed evolution and bar reformation" Memorie della Societa Astronomica Italiana Supplement, v.18, p.53

[25] de Lorenzo-Cáceres, A. et al. 2019 "Clocking the assembly of double-barred galaxies with the MUSE TIMER project" Monthly Notices of the Royal Astronomical Society, Volume 484, Issue 4, p.5296-5314

[26] de Lorenzo-Cáceres, A. et al. 2013 "Distinct stellar populations in the inner bars of double-barred galaxies" Monthly Notices of the Royal Astronomical Society, Volume 431, Issue 3, p.2397-2418

[27] Donohoe-Keyes, C.E. et al. 2019 "Redistribution of stars and gas in the star formation deserts of barred galaxies" Monthly Notices of the Royal Astronomical Society, Volume 489, Issue 4, p.4992-5003

[28] Eggen, O.J. et al. 1962 "Evidence from the motions of old stars that the Galaxy collapsed." Astrophysical Journal, vol. 136, p. 748

[29] Elmegreen, B.G. et al. 2008 "Bulge Formation by the Coalescence of Giant Clumps in Primordial Disk Galaxies" The Astrophysical Journal, Volume 688, Issue 1, pp. 67-77

[30] Erwin, P. et al. 2005 "Antitruncation of Disks in Early-Type Barred Galaxies" The Astrophysical Journal, Volume 626, Issue 2, pp. L81-L84.

[31] Falcón-Barroso, J. et al. 2015 "Angular Momentum across the Hubble sequence from the CALIFA survey" Galaxy Masses as Constraints of Formation Models, Proceedings of the International Astronomical Union, IAU Symposium, Volume 311, pp. 78-81

[32] Falcón-Barroso, J. et al. 2011 "An updated MILES stellar library and stellar population models" Astronomy & Astrophysics, Volume 532, id.A95, 8 pp.

[33] Fall, S. M. & Efstathiou, G. 1980 "Formation and rotation of disc galaxies with haloes" Monthly Notices of the Royal Astronomical Society, Vol. 193, 189-206

[34] Ferrers, N. M. 1877, Quart. J. Pure and Appl. Math, 14, 1

[35] Freeman, K.C, 1970 "On the Disks of Spiral and S0 Galaxies" Astrophysical Journal, vol. 160, p.811

[36] Gadotti, D.A. 2009 "Structural properties of pseudo-bulges, classical bulges and elliptical galaxies: a Sloan Digital Sky Survey perspective" Monthly Notices of the Royal Astronomical Society, Volume 393, Issue 4, pp. 1531-1552

[37] Gadotti, D.A. 2008 "Image decomposition of barred galaxies and AGN hosts" Monthly Notices of the Royal Astronomical Society, Volume 384, Issue 1, pp. 420-439.

[38] García-Lorenzo, B. et al. 2015 "Ionized gas kinematics of galaxies in the CALIFA survey. I. Velocity fields, kinematic parameters of the dominant component, and presence of kinematically distinct gaseous systems" Astronomy & Astrophysics, Volume 573, id.A59, 43 pp.

[39] González-Delgado, B. et al. 2017 "Spatially-resolved star formation histories of CALIFA galaxies. Implications for galaxy formation" Astronomy & Astrophysics, Volume 607, id.A128, 21 pp.

[40] González-Delgado, B. et al. 2016 "Star formation along the Hubble sequence. Radial structure of the star formation of CALIFA galaxies" Astronomy & Astrophysics, Volume 590, id.A44, 17 pp.

[41] González-Delgado, B. et al. 2015 "Insights on the Stellar Mass-Metallicity Relation from the CALIFA Survey"The Astrophysical Journal Letters, Volume 791, Issue 1, article id. L16, 5 pp.

[42] González-Delgado, B. et al. 2014 "Insights on the Stellar Mass-Metallicity Relation from the CALIFA Survey"The Astrophysical Journal Letters, Volume 791, Issue 1, article id. L16, 5 pp.

[43] Graham, A.W. and Driver, S.P. 2005 "A Concise Reference to (Projected) Sérsic R1/n Quantities, Including Concentration, Profile Slopes, Petrosian Indices, and Kron Magnitudes" Publications of the Astronomical Society of Australia, Volume 22, Issue 2, pp. 118-127.

[44] Hathi, N. P. et al. 2009 "Stellar Populations of Late-Type Bulges at z $\simeq$ 1 in the Hubble Ultra Deep Field" The Astrophysical Journal, Volume 690, Issue 2, pp. 1866-1882

[45] Hopkins, P.F. 2009 "Dissipation and Extra Light in Galactic Nuclei. II. "Cusp" Ellipticals" The Astrophysical Journal Supplement, Volume 181, Issue 1, pp. 135-182

[46] James, P. A. & Percival, S. M. 2016 "The Hα galaxy survey. VII. The spatial distribution of star formation within disks and bulges" Astronomy and Astrophysics, Volume 501, Issue 1, 2009, pp.207-220

[47] James, P. A. et al. 2009 "Stellar population constraints on the ages of galactic bars" Monthly Notices of the Royal Astronomical Society, Volume 457, Issue 1, p.917-925

[48] Kauffmann, G. 1996 "The age of elliptical galaxies and bulges in a merger model" Monthly Notices of the Royal Astronomical Society, Volume 281, Issue 2, pp. 487-492.

[49] Khoperskov, S. et al. 2018 "Bar quenching in gas-rich galaxies" Astronomy & Astrophysics, Volume 609, id.A60, 17 pp.

[50] Laurikainen, E et al. 2005 "Multicomponent decompositions for a sample of S0 galaxies" Monthly Notices of the Royal Astronomical Society, Volume 362, Issue 4, pp. 1319-1347.

[51] Madau, P. & Dickinson, M. 2014 "Cosmic Star-Formation History" Annual Review of Astronomy and Astrophysics, vol. 52, p.415-486

[52] Masters, K. L. et al. 2012 "Galaxy Zoo and ALFALFA: atomic gas and the regulation of star formation in barred disc galaxies" Monthly Notices of the Royal Astronomical Society, Volume 424, Issue 3, pp. 2180-2192.

[53] Méndez-Abreu,J. et al. 2019 "Spectro-photometric decomposition of galaxy structures" Monthly Notices of the Royal Astronomical Society, Volume 484, Issue 3, p.4298-4314

[54] Méndez-Abreu, J. et al. 2019 "Inner bars also buckle. The MUSE TIMER view of the double-barred galaxy NGC 1291" Monthly Notices of the Royal Astronomical Society: Letters, Volume 482, Issue 1, p.L118-L122

[55] Méndez-Abreu, J. et al. 2018 "The intrinsic three-dimensional shape of galactic bars" Monthly Notices of the Royal Astronomical Society, Volume 479, Issue 3, p.4172-4186

[56] Méndez-Abreu, J. et al. 2017 "Two-dimensional multi-component photometric decomposition of CALIFA galaxies" Astronomy & Astrophysics, Volume 598, id.A32, 18 pp.

[57] Méndez-Abreu, J. et al. 2014 "Secular- and merger-built bulges in barred galaxies" Astronomy & Astrophysics, Volume 572, id.A25, 16 pp.

[58] Méndez-Abreu, J. et al. 2008 "Structural properties of disk galaxies. I. The intrinsic equatorial ellipticity of bulges" Astronomy and Astrophysics, Volume 478, Issue 2, February I 2008, pp.353-369

[59] Neumann, J. et al. 2020 "Stellar populations across galaxy bars in the MUSE TIMER project" Astronomy & Astrophysics, Volume 637, id.A56, 28 pp.

[60] Oh, Seulhee et al. 2012 "Bar Effects on Central Star Formation and Active Galactic Nucleus Activity" The Astrophysical Journal Supplement, Volume 198, Issue 1, article id. 4, 13 pp.

[61] Pérez, E. et al. 2013 "The Evolution of Galaxies Resolved in Space and Time: A View of Inside-out Growth from the CALIFA Survey" The Astrophysical Journal Letters, Volume 764, Issue 1, article id. L1, 6 pp.

[62] Pohlen, M. and Trujillo, I. 2006 "The structure of galactic disks. Studying late-type spiral galaxies using SDSS" Astronomy and Astrophysics, Volume 454, Issue 3, August II 2006, pp.759-772

[63] Prieto, M. et al. 2001 "Optical surface photometry of a sample of disk galaxies. II. Structural components" Astronomy and Astrophysics, v.367, p.405-427

[64] Quillen, Alice C. et al. 2014 "A vertical resonance heating model for X- or peanut-shaped galactic bulges" Monthly Notices of the Royal Astronomical Society, Volume 437, Issue 2, p.1284-1307

[65] Robichaud, F. et al. 2017 "Star formation history in barred spiral galaxies - active galactic nucleus feedback" Monthly Notices of the Royal Astronomical Society, Volume 469, Issue 3, p.3722-3737

[66] Salo, Heikki et al. 2015 "The Spitzer Survey of Stellar Structure in Galaxies (S4G): Multi-component Decomposition Strategies and Data Release" The Astrophysical Journal Supplement Series, Volume 219, Issue 1, article id. 4, 45 pp.

[67] Sánchez, S. F. et al. 2016 "CALIFA, the Calar Alto Legacy Integral Field Area survey. IV. Third public data release" Astronomy & Astrophysics, Volume 594, id.A36, 21 pp.

[68] Sánchez, S. F. et al. 2012 "CALIFA, the Calar Alto Legacy Integral Field Area survey. I. Survey presentation" Astronomy & Astrophysics, Volume 538, id.A8, 31 pp.

[69] Sánchez-Blázquez, P. et al. 2014 "Stellar population gradients in galaxy discs from the CALIFA survey. The influence of bars" Astronomy & Astrophysics, Volume 570, id.A6, 85 pp.

[70] Sánchez-Blázquez, P. et al. 2006 "Medium-resolution Isaac Newton Telescope library of empirical spectra" Monthly Notices of the Royal Astronomical Society, Volume 371, Issue 2, pp. 703-718.

[71] Seidel, M. K. et al. 2016 "The BaLROG project - II. Quantifying the influence of bars on the stellar populations of nearby galaxies" Monthly Notices of the Royal Astronomical Society, Volume 460, Issue 4, p.3784-3828

[72] Sérsic, J.L. 1968 "Atlas de Galaxias Australes" Cordoba, Argentina: Observatorio Astronomico, 1968

[73] Sellwood, J. A. and Gerhard, Ortwin 2020 "Three Mechanisms for Bar Thickening" Monthly Notices of the Royal Astronomical Society, Advance Access

[74] Sheth, Kartik et al. 2012 "Hot Disks and Delayed Bar Formation" The Astrophysical Journal, Volume 758, Issue 2, article id. 136, 7 pp.

[75] Sheth, Kartik et al. 2008 "Evolution of the Bar Fraction in COSMOS: Quantifying the Assembly of the Hubble Sequence" The Astrophysical Journal, Volume 675, Issue 2, pp. 1141-1155

[76] Trujillo, Ignacio et al. 2007 "Strong size evolution of the most massive galaxies since z $\simeq$ 2" Monthly Notices of the Royal Astronomical Society, Volume 382, Issue 1, pp. 109-120.

[77] van Dokkum, Pieter G. et al. 2010 "The Growth of Massive Galaxies Since z = 2" The Astrophysical Journal, Volume 709, Issue 2, pp. 1018-1041

[78] Vazdekis, A. et al. 2010 "MILES SSP Models" Vazdekis, A.; Sánchez-Blázquez, P.; Falcón-Barroso, J.; Cenarro, A. J.; Beasley, M. A.; Cardiel, N.; Gorgas, J.; Peletier, R.

[79] Vera, Matias et al. 2016 "Effect of bars on the galaxy properties" Astronomy & Astrophysics, Volume 595, id.A63, 10 pp.

[80] Weinzirl, T. et al. 2009 "Bulge n and B/T in High-Mass Galaxies: Constraints on the Origin of Bulges in Hierarchical Models" The Astrophysical Journal, Volume 696, Issue 1, pp. 411-447

[81] Woo-Young, Seo et al. 2019 "Effects of Gas on Formation and Evolution of Stellar Bars and Nuclear Rings in Disk Galaxies" The Astrophysical Journal, 872:5 (22pp)

[82] Wozniak, Hervé 2015 "How can double-barred galaxies be long-lived?" Astronomy & Astrophysics, Volume 575, id.A7, 14 pp.